Chapter 12

Downhole Applications of Geophysics

Frederick L. Paillet[1] *and Karl J. Ellefsen*[2]

Introduction

Many geotechnical, environmental, and hydrological investigations require information about soil, sediments, bedrock and groundwater. Boreholes are drilled to investigate these materials in the subsurface, and borehole geophysical measurements are one of the primary methods for determining subsurface properties. Borehole geophysics provides measurements of subsurface properties under in-situ conditions, with no missing samples, and using several different physical measurements. Some of these measurements can be directly linked to noninvasive surface soundings, and a number of new borehole geophysical techniques are under development.

In this chapter, geophysical well logging is defined as the measurement and the analysis of physical properties when the measurement is made with equipment in one or more boreholes. This broad definition of borehole geophysics includes many different measurements. As shown in Figure 1, these measurements can be divided into four basic types: (1) Conventional wireline logging (borehole geophysics, Figure 1a). The distinguishing feature of this type is that all equipment that is used to make the measurement is within one borehole. Some common examples of this type are acoustic-velocity and electrical-resistivity logging. (2) Direct push geophysics (Figure 1b). For this type, all measurement equipment is also within one borehole, although the borehole is not drilled before logging. Instead, the borehole is made by a steel rod as it is pushed into unconsolidated soils and sediments (overburden). The measurement sensors are located on or near the tip of the rod. The measured physical properties may include pressure on the rod tip and electrical resistivity. (3) Surface to borehole geophysics (Figure 1c). The distinguishing feature of this type is that some of the measurement equipment is on the ground surface, and the rest is in a borehole. A common example is vertical seismic profiling (VSP), for which the seismic source is on the ground surface and the seismic receivers are in the borehole. (4) Borehole to borehole geophysics (Figure 1d). For this type, measurement equipment is in two different boreholes. An example is borehole to borehole (crosswell) radar, for which the transmitting antenna is in one borehole and the receiving antenna in another.

Geotechnical and hydrological investigations often include conventional logging and direct push logging. One reason for their frequent use is that these two types of logging are usually cheaper than extracting core during drilling. In addition, the logging measurements can be made along the entire borehole and can be orientated using a magnetometer, whereas core may not be extracted from some depth intervals because of fracturing (in rock) or very poor consolidation (in sediments), and the azimuthal orientation of core is usually unknown. Another reason for their frequent use is that the logging measurements are usually repeatable, even with different equipment and equipment operators. In contrast, drillers' logs are comparatively less repeatable because their accuracy depends upon the expertise of the driller. Because of the repeatability of logging measurements, they can be used to monitor changes with time—for example, changes related to the migration of aqueous contaminants.

Surface-to-borehole and borehole-to-borehole geophysics are used to measure physical properties away from the borehole, usually beyond the region that can be measured with conventional logging equipment. When the objective of an investigation is in bedrock, borehole-to-borehole geophysics may provide images with high spatial resolution, because the measurements are unaffected by the overburden. Surface-to-borehole geophysics is often useful in interpreting surface data. For example, seismic sections from vertical seismic profiling data and surface seismic data may be compared. If the correlation is good, then reflecting horizons in the surface seismic data can be tied to lithologic contacts or fracture zones that occur at known depths in the borehole. However, surface-to-borehole methods, such as VSP, involve scales of investigation and data processing techniques that are a logical extension of closely related surface sounding technique and are discussed in chapters dealing with those methods (see Chapter 6).

Because of the large number of techniques used in borehole geophysics, a complete discussion of these tech-

[1]Department of Earth Sciences, University of Maine, Orono, ME, 04469-5790. E-mail: fpaillet@maine.edu.

[2]U. S. Geological Survey, MS 964, Box 25046, Federal Center, Lakewood, CO 80225. E-mail: ellefsen@usgs.gov

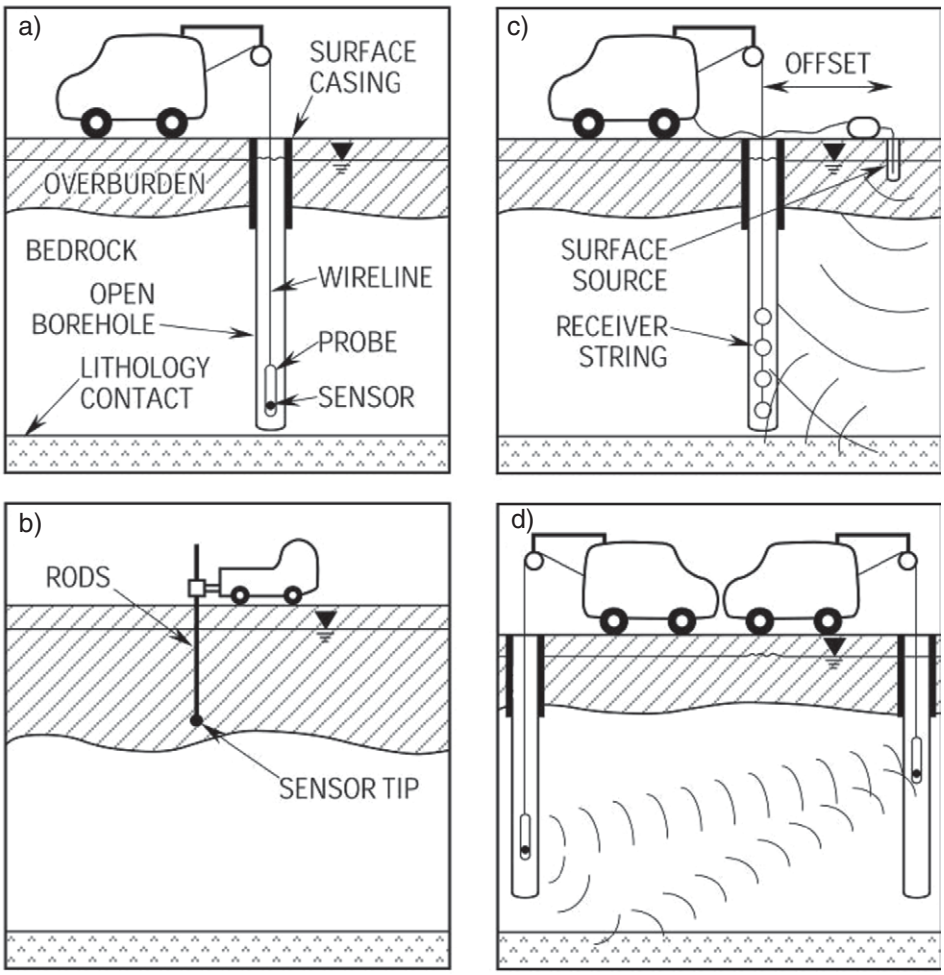

Figure 1. Schematic illustration of four different classes of geophysical measurements in boreholes: (a) conventional wireline well logging; (b) direct push technology where sensors are driven into the subsurface using rigid rods; (c) surface to borehole measurements where the scale of investigation allows relatively large separations between borehole measurements stations and where lithologic features beyond the borehole may be detected; and (d) borehole-to-borehole measurements used to characterize formations between boreholes, but features outside the plane of investigation can contribute to the measurements.

niques would require at least an entire book. To keep the discussion concise, this chapter is restricted to an introduction to the most commonly used techniques. The intent is that readers will use this chapter to learn the basic principles underlying the various techniques. Readers can get more information about the techniques from the references. In addition, some references for those borehole geophysical techniques that are less common are listed.

Geophysical measurements of several different varieties (Table 1) commonly are made in open or cased boreholes. These measurements are approximately analogous to geophysical soundings made on the land surface, except that the measurements are made along the inside surface of a borehole (Figure 2; Paillet et al., 1999a). The greatest difference between the surface and borehole measurements is that the scale of the surface measurements is systematically increased to reach greater depths of investigation, whereas the borehole measurements are made at the same, generally much smaller, scale at various depths along the borehole. A geophysical well log is the profile produced by recording the geophysical response as a function of depth as the logging probe is moved along the well bore. Such measurements are routinely used to define the stratigraphy and structure of geologic formations where core is not recovered, or where core recovery is incomplete. Borehole geophysical measurements can also be used for comparison with surface geophysical soundings made at the same location, as, for example, in converting the two-way traveltime scale of surface seismic reflections to true depth below land surface. Although the borehole geophysical measurements described in this chapter provide tremendous help in characterizing the subsurface in geotechnical, groundwater, and environmental studies, a number of new and improved borehole logging techniques are under development. Some of the most important of these are listed in Table 2. A glossary of technical terms related to borehole geophysics is given by SPWLA (1975). Useful general references on borehole geophysics are ASTM (1995), Brock (1986), Doveton (1986), Ellis (1987), Hearst et al. (2000), Hurst et al. (1990), and Keys (1990).

General Background

Borehole geophysical measurements can be made with the geophysical sensors lying along the borehole wall so that the measurement is directed along one side, or with the sensors centralized within the borehole so that geophysical response is averaged over the full azimuth as indicated in

Figure 2. In either situation, the measurement is designed so that the geophysical response is derived from an approximately spherical region surrounding the nominal depth position of the borehole sensors. The sphere is identified as the sampled volume that contributes about 90% of the total measured response in the convolution integral:

$$G = \int_0^R \int_0^{2\Pi} \int_0^{2\Pi} g(r,\phi,\theta)\ d\phi\ d\theta\ dr, \qquad (1)$$

where $g(r, \phi, \theta)$ is the actual distribution of the geophysical quantity in the region around the nominal measurement depth. The radius of the sample volume is designated as the value of R at which the integral achieves 90% of the value that would result if the integration were extended to the limit $R \rightarrow \infty$. The diameter of the sample volume determines the vertical resolution of the log. The sample volume of geophysical logging equipment is usually designed to provide an effective compromise between the need to minimize the effects of the borehole environment on the measurement and the need to maximize vertical resolution. That is, the volume of investigation needs to be large enough such that the borehole and casing and annulus (if present) do not contribute in a disproportionate way to the composite measurement and yet small enough to insure effective resolution of thin beds. Standard geophysical logging probes are designed with sample volumes of from two to four borehole diameters, with specific probes intended for groundwater and environmental applications (5.0–15.0 cm diameter boreholes) and oil-field applications (15.0–25.0 cm diameter boreholes).

Geophysical logs are usually obtained using a self-contained logging truck equipped with winch, depth control system, and computerized operating system (Figure 3). Depth control is provided by a measuring wheel such that friction of the logging cable on the wheel generates pulses that can be correlated with the rate of movement of the probe along the borehole. Slip rings on the winch allow power supply to the probe and communication of data streams to the uphole computer. The logging truck is either equipped with a boom that can be positioned directly over the wellhead, or the cable is run through a sheave wheel suspended over the top of casing. Older logging systems that may still be in operation record analog data on strip charts, but most modern logging equipment is controlled by a PC-based operating system with data digitally recorded on a disk. An important feature of the logging operation is that several different geophysical measurements can be made by connecting different probes to the same winch and operating system. In fact, some logging probes are capable of making more than one measurement on a single pass along the borehole. An example of a suite of log measurements is shown for typical sedimentary rocks in Figure 4. The ease with which widely different physical measurements, such as gamma activity, neutron attenuation, and acoustic traveltime, can be run off of the same equipment is a unique and useful aspect of geophysical logging.

General Concepts of Borehole Geophysics

A geophysical log consists of two quantities: measurement depth and geophysical response. The value of the log depends on the accuracy of both of these quantities. That is, a highly accurate measurement of the geophysical response of a certain subsurface bed is not useful if that measurement is identified with an adjacent bed because of a depth error in the log (Paillet and Crowder, 1996; Keys, 1986). Therefore, quantitative geophysical log interpretation involves analysis of depth values as well as the geophysical measurement assigned to a certain depth. The depth scales on individual logs are routinely adjusted by crosscorrelation with other logs from the same borehole to insure that deflections associated with beds (Figure 4) occur at the same depth on all logs. Many modern probes contain gamma detectors so that gamma logs obtained on separate runs can be used for depth correlation of logs. The depth scale is further verified by insuring that the nominal zero depth point is achieved at the end of the logging run and that sections of logs repeat in the field (ASTM, 1995).

After routine verification of depth scales and adjustment of depth scale for individual logging runs by crosscorrelation, log analysis is based on four general attributes of this class of data (Paillet and Crowder, 1996):

1) Logs provide a continuous depth profile of the physical properties of the geologic formation adjacent to the borehole.
2) Logs sample a finite volume of undisturbed formation saturated with natural fluids in an annular region surrounding the borehole.
3) Logs measure physically independent properties that can be represented in terms of several different variables.
4) Logs can be used to generate regressions between geophysical quantities and geochemical or hydraulic measurements based on core samples or straddle-packer tests.

Effective log analysis and interpretation are based on achieving the full potential of these four fundamental attributes of borehole geophysics.

Depth profile

Geophysical logs generally measure a physical property such as gamma activity or acoustic traveltime that is only

Table 1. Summary of conventional geophysical logs and their applications in the shallow subsurface (from Paillet and Crowder, 1996).

Type of log	Varieties and related techniques	Properties measured	Potential application	Required hole conditions	Other limitations
Spontaneous potential		Electric potential caused by salinity differences in borehole and interstitial fluids	Lithology, shale content, water quality	Uncased hole filled with conductive fluid.	Salinity difference needed between borehole fluid and interstitial fluids
Single-point resistance	Conventional, differential	Resistance of rock, saturating fluid, and borehole fluid	High-resolution lithology, fracture location by differential probe	Uncased hole filled with conductive fluid	Not quantitative; hole diameter effects significant
Multielectrode resistivity	Normal, focused, or lateral	Resistivity, in ohm-meters, of rock and saturating fluids	Quantitative data on salinity of interstitial water; lithology	Uncased hole filled with conductive fluid	Normals provide incorrect values and thicknesses in thin beds
Electrical induction	Deep, shallow, and focused	Resistivity, in ohm-meters, of rock and saturating fluids	Quantitative data on salinity of interstitial water; lithology	Open hole with plastic casing	Skin effect correction for highly conductive formation
Natural gamma	Gamma spectral	Gamma radiation from natural or artificial isotopes	Lithology—may be related to clay and silt content and permeability; spectral identifies radioisotopes	Any hole conditions, except very large, or several strings of casing and cement	Very high counts need to be corrected for dead-time
Gamma-gamma	Compensated (dual detector)	Electron density	Bulk density, porosity, moisture content, litholog	Optimum results in uncased; qualitative through casing or drill stem	Severe hole-diameter effects
Neutron	Epithermal, thermal, compensated activation, pulsed	Hydrogen content	Saturated porosity, moisture content, activation analysis, lithology	Optimum results in uncased; can be calibrated for casing	Hole-diameter and chemical effects
Acoustic velocity	Compensated waveform	Compressional wave velocity	Porosity, lithology, fracture location and character, cement bond	Fluid-filled, 3 to 16-in diameter	Does not see secondary porosity
Acoustic televiewer	Acoustic caliper	Acoustic reflectivity of borehole wall	Location, orientation, and character of fractures and solution openings, strike and dip of bedding, casing inspection	Fluid-filled	Heavy mud or mud cake attenuate signal; very slow log

Table 1. Summary of conventional geophysical logs and their applications in the shallow subsurface (from Paillet and Crowder, 1996). *(cont.)*

Type of log	Varieties and related techniques	Properties measured	Potential application	Required hole conditions	Other limitations
Caliper	Oriented, 4-arm high-resolution bow spring	Hole or casing diameter	Hole-diameter corrections to other logs, lithology, fractures, hole volume for cementing	Any conditions	Deviated holes limit some
Fluid column temperature	Differential	Temperature of fluid near sensor	Geothermal gradient, in-hole flow, location of injected water, correction of other logs, curing cement	Fluid-filled	Accuracy and resolution of tool varies
Fluid column conductivity	Resistivity	Most measure resistivity of fluid in hole	Quality of borehole fluid, in-hole flow, location of contamination plumes	Fluid-filled	Accuracy varies, requires temperature correction
Flow	Spinner, tracer, thermal pulse, electro-magnetic	Velocity of net flow in borehole	In-hole flow, location, and apparent hydraulic conductivity of permeable interval	Fluid-filled	Spinners require higher velocities. Needs to be centralized

indirectly related to physical properties of interest, such as mineralogy, mechanical strength, or fluid-filled porosity. In contrast, samples such as cuttings or cores recovered during drilling provide direct evidence of the geological properties of the formation, but these samples are affected by drilling fluid, damaged by mechanical processes, and subject to discontinuous recovery. The first important step in the analysis of geophysical logs is the correlation between descriptions of cuttings or core and the geophysical logs. The combination of both physical description and continuous geophysical logs is used to formulate the interpretation problem so that a given set of log responses can be related to a specified lithologic unit or other feature as indicated by the example in Figure 4. In the figure, direct physical inspection of cuttings is expressed as relative coarseness of sediments, while the logs are used to identify the tops and bottoms of fine-grained sedimentary units interpreted as confining units for a hydrogeologic study.

Finite sample volume

Geophysical logs also allow interpretation of the properties of undamaged formations saturated with natural groundwater. Identification of the volume sampled by each measurement and correction of that measurement for the effects of the fluid filled borehole and casing within the sampled volume are important in log analysis. In Figure 4, for example, the resistivity values given by the short normal log must be corrected for the effects of borehole drilling-mud conductivity to give an estimate of formation electrical resistivity or conductivity.

Multiple geophysical measurements

Geophysical logging systems are equipped with sensors for several different measurement types that can be interpreted by mathematically independent interpretation equations. Most geophysical interpretation problems

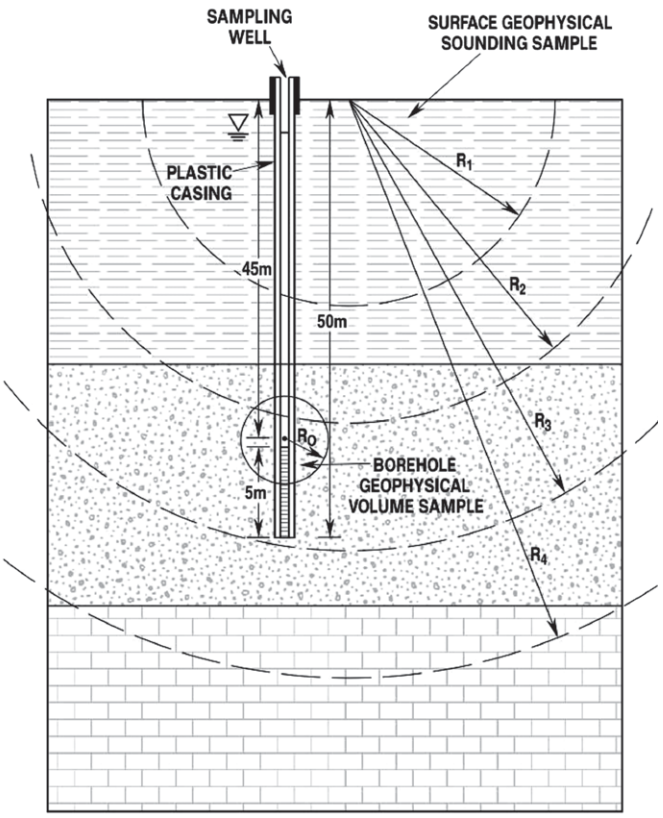

Figure 2. Sample volumes associated with surface and borehole geophysics, compared to sampling and hydraulic test environment for a typical observation well used in groundwater studies (from Paillet et al., 1999a).

involve several unknown parameters, such as rock type, water salinity, porosity, and permeability. Physically independent measurements can be treated as sets of coupled interpretation equations. In theory, these are coupled linear equations that can be solved by elimination of variables (Doveton, 1986). In practice, the interpretation equations are slightly nonlinear, and solutions are based on numerical methods used in iterations to find the intersection of these curves in parameter space.

Regression

Boreholes provide access to the subsurface in a way that allows regression of geophysical measurements against physical or hydraulic properties of interest. In a very simple example, specific capacity tests could be used to estimate the permeability of the open interval in a series of observation wells. Then the gamma log, qualitatively correlated with the fine-grained fraction of sediments in the formation, can be given a quantitative permeability scale (Keys, 1986, 1990).

Quantitative Log Inversion

Much of geophysical well log analysis is based on a strictly qualitative analysis of the log data, where bed boundaries are picked, and general lithologies described for each bed (Figure 4). Such an analysis is quantitative only in that precise depths are assigned for bed contacts.

Table 2. Summary of new logging technology under development or already available for oil-field applications, and projected to be available for groundwater, environmental, and engineering applications in the near future.

Log	Measurement	Application	Reference
Nuclear magnetic resonance	Nuclear magnetic moment	Detection of moveable hydrogen (water)	Kenyon, 1997
Mineral activation	Gamma spectral response after neutron activation	Mineral identification in situ	Jacobsen et al., 1993
Dielectric	High-frequency response to electromagnetic signal	Fluid and mineral identification using dielectric properties	Gilmore et al., 1987
Tunable acoustic	Acoustic propagation at variable frequency	Mechanical and fluid properties	Oden et al., 2000
High-resolution gamma spectral	Identify energy levels of natural gamma	Lithology and clay mineral typing	Lofts et al., 1993
Ion specific fluid log	Specific ions with special detectors	Water chemistry	Rossi and Peroni, 1989
Wireline packer	Differential pressure in isolated interval	Permeability and water chemistry	Paillet et al., 1999b
Horizontal flow	Three-dimensional flow in situ	Contaminant dispersal	Newhouse and Hansen, 2000; Kearal, 1997

This assignment is made using the half-amplitude deflection rule, where the contact between two beds is fixed at the depth point where the log attains a value exactly half way between the average values within each bed (Hearst et al., 2000; Keys, 1990). There are exceptions to this rule, such as normal and laterolog resistivity measurements, where the log response is a complicated function of probe position relative to bed boundaries and the precise location of bed boundaries requires additional analysis (Lynch, 1962). Fully quantitative analysis results in the assignment of numerical values to the lithologic, mechanical, or hydrogeologic properties of the beds. Such analysis is restricted to logs where the geophysical measurement can be identified with the volume-averaged properties of a specific sample volume (Paillet and Crowder, 1996; Doveton, 1986). Gamma and resistivity logs provide such measurements, whereas caliper and borehole-wall image logs do not.

The geophysical responses given by each log are assumed to be related to physical properties of interest through equations of the form,

$$G_i = C_0 + C_1 X_1 + C_2 X_2 + \ldots + C_N X_N; \quad i = 1, 2, 3, \ldots M, \tag{2}$$

where G_i is the log data from log index i, the X_j are N different formation parameters of interest, and the C_j are calibration constants relating the measurement to parameter X_j.

Although the general form of these equations is based on theory, the constants are derived from borehole or core sample regression performed under carefully controlled circumstances. In each such set of relations, M geophysical measurements are assumed to be linearly related to N different formation properties. We generally expect that $N > M$. In practice, however, we use principle components analysis or some other technique to limit the number of unknowns to the few most important parameters, such as effective porosity or clay mineral fraction. If $M = N$, then the equations can be solved by matrix methods or elimination of variables. Often the equations between the G_i and the X_j are found to be slightly nonlinear. This is not a real problem, because the initial parameter guess is assumed to be close enough to a solution that numerical iteration can find the point of intersection of the interpretation equations in parameter space.

In principle, the quantitative analysis of geophysical logs appears to depend upon the ability to reduce the N possible parameters to a set of M quantities such that the M coupled equations can be solved numerically for M unknowns. In practice, the solution is confounded by the fact that the constants that appear in the equations also are not well defined. The solution is constrained further by restricting the variables such that $M > N$. In that situation, the solution is over-determined. For example, if $M = N + 1$, then the first N of the M equations can be solved. The solution vector generally will not exactly satisfy the last equation. That is, the value given for the G_M by substitution of the X_j into the Mth equation will not equal the measured value. The mean square difference can be treated as a residual to be minimized by systematically varying the C_j to find the best possible fit to the full set of measurements (Parker, 1994). This technique is essentially the same as the residual minimization used in most other geophysical inversion methods (see Chapter 4). A specific example of the quantitative inversion of geophysical well logs is given in Appendix A.

Figure 3. A typical logging truck used in shallow subsurface investigations; the truck is equipped with 1500 m of wireline, winch, generator, digitally controlled operating system, and probes capable of making most of the geophysical measurements listed in Table 1.

Examples of Typical Conventional Well Logs

Gamma log

One of the simplest and most commonly used well logs is the gamma log. This log measures the total gamma emission produced by naturally occurring isotopes of potassium, thorium, and uranium. The gamma activity of a geological formation is assumed to depend on lithology, although there is no universal one-to-one mapping between gamma activity and rock or sediment type (Figure 4). Gamma spectral logging systems count gammas within certain narrow energy windows that can be related to daughter radioisotopes in one of the three radioisotope series, but available gamma spectral logging equipment for

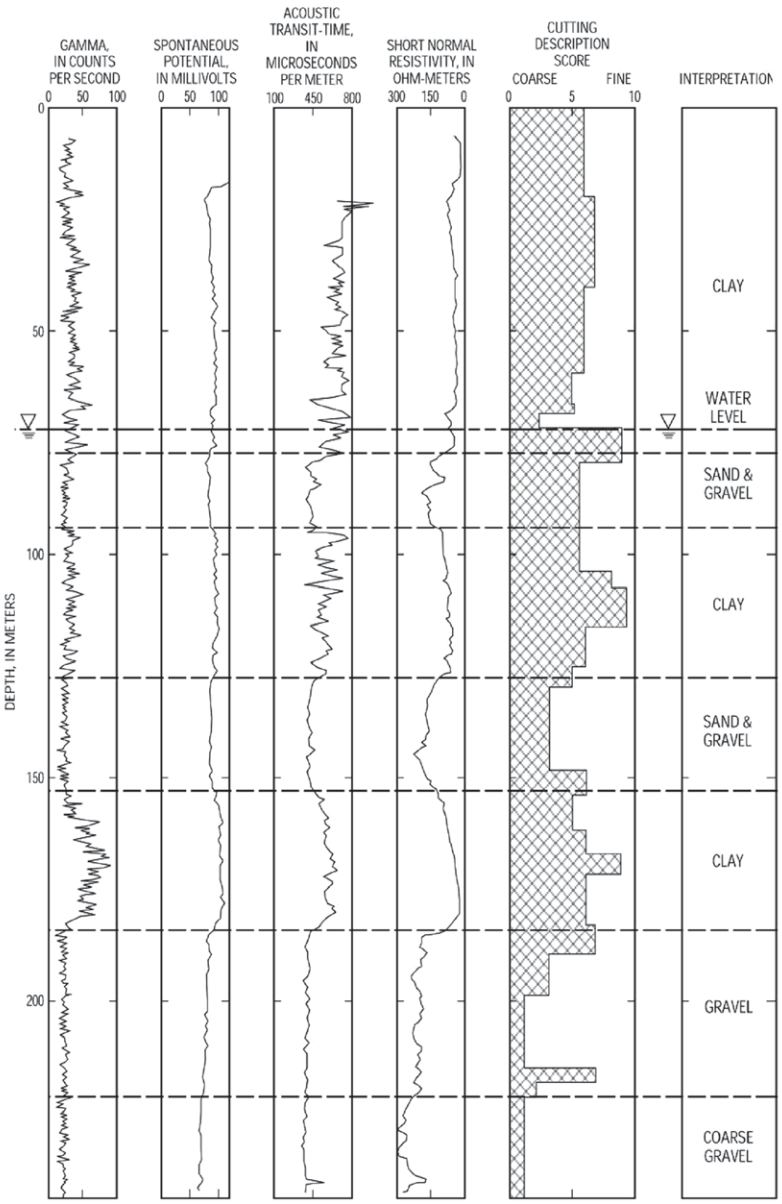

Figure 4. Example of several different geophysical logs obtained in an alluvial basin in Nevada illustrating how individual logs are depth correlated, and showing the interpretation of sediment type and thickness based on the combination of geophysical logs and lithologic description derived from drill cuttings (Paillet and Crowder, 1996).

slim boreholes has relatively poor resolution and counting statistics. It is commonly assumed that total gamma activity as given by gamma logs increases with volume percent of the clay mineral fraction in unconsolidated sediments (Keys, 1990; Wahl, 1983). A typical example of a gamma log used in groundwater monitoring is illustrated in Appendix B.

One of the important limitations on gamma logs is imposed by nuclear statistics. Gamma activity at a certain depth in the borehole has to be averaged over a counting period to give a true reading of average gamma activity (Keys, 1990). In practice, this means that the gamma log must be run slowly enough that the filtering of the log data needed to suppress nuclear statistical noise does not degrade the vertical resolution. The simplest way to verify that nuclear statistical noise has been properly suppressed without degrading vertical resolution is to repeat a section of log. An example is illustrated in Appendix C.

One of the most important applications of gamma logging is as a stratigraphic control technique (Figure 5). In this example, gamma logs from three different boreholes are used to define the stratigraphic strike and dip of sedimentary rock in northwestern Illinois. Standard crosscorrelation techniques are used to define the depth alignment for maximum correlation between the three traces. Then, wellhead elevations can be used to define the elevations of marker strata at each borehole location. The elevations where these beds intersect each borehole can then be used to define the regional strike and dip of the sedimentary section.

Other nuclear logs

There are other nuclear logs besides the gamma log, but the two most prominent of these, neutron porosity and gamma-gamma density logs, require use of a radioactive source. This imposes cumbersome licensing requirements on the user and serious logistical problems relating to well access. Even so, these logs sometimes provide critical information for a specific study, and the logs can be obtained as a service from various commercial contractors. The neutron log measures the flux of neutrons scattered back to one or more detectors located a given distance along the probe from the source. The density log makes a similar measurement using two gamma detectors. Each of these probes generates measurements given in counts per second from one or two detectors. These count rates are then calibrated in controlled environments to generate regressions between count rates and water-filled porosity (in percent) for the neutron log and between count rates and mass density (in g/cm^3) for the density log (Hodges, 1988). One important consideration in neutron or density log interpretation is that either log can be difficult to interpret on its own. Neutron porosity logs do not distinguish between the effective (that is, drainable) porosity of interest to hydrologists and the noneffective porosity attributed to water bound to clay minerals. Porosity estimated from a density log

depends on the mineral-grain density assumed for the matrix. Most effective interpretation of neutron porosity and gamma-gamma density logs results when other logs are used to adjust nuclear-log response to account for the effects of bound water and mineral-grain density.

Electric log

Electric logs of various kinds are used to measure the electrical conductivity of the formation surrounding the borehole (Pirson, 1963). Electric logs can be divided into three general classes: (1) induction logs using low frequency signals (typically in the range 10–40 kHz) to measure the conductivity of a toroid-shaped volume surrounding the borehole; (2) "normal" logs analogous to scaled-down Schlumberger DC array measurements that are influenced by formation and borehole fluid; and (3) fluid column measurements sampling the electrical conductivity of the borehole fluid column. The electrical conductivity of geologic formations is usually assumed to consist of the sum of conductivity along parallel current paths, one through networks of pores and the other through the mineral grains in contact. Thus, formation conductivity is expressed in the form (Jorgensen, 1991; Kwader, 1985),

$$\sigma = \sigma_0 + \frac{\sigma_W}{F}, \tag{3}$$

where σ is the formation conductivity, σ_0 is the conductivity of the mineral grain matrix, σ_w is the conductivity of the pore water, and F is the formation factor. For most logging applications, F is assumed to be an intrinsic property of the aquifer. In the limit of nonconducting mineral grains such as quartz, the formation factor reduces to

$$F = \frac{\sigma_W}{\sigma}. \tag{4}$$

In natural rock formations, the assumption of constant F only holds true in the limit of relatively large values of σ_w (about 1000 μS/cm or greater; Biella et al., 1983). When electrically insulating minerals are saturated with relatively fresh water, various surface conduction mechanisms become important at the interface of mineral and water in the pore spaces, and F cannot be treated as a simple constant for a given rock type.

A typical induction log in unconsolidated carbonate sediments is illustrated in Figure 6 (Paillet and Reese, 2000). The drilling report and other log data indicate that sediments are composed of quartz and carbonate grains with no clays, so that all of the electrical conductivity of the formation is accounted for by conduction through pore spaces. The induction log shows two "steps" related to shifts in pore water salinity as the borehole breaches confining units in the aquifer. The induction log is automatically corrected in the logging software for skin effects and is completely unaffected by the electrical conductivity of the borehole fluid (drilling mud).

In most applications, formation electrical conductivity (or its inverse, resistivity) will vary as a function of lithology, pore structure, and pore water salinity (Figure 7; Paillet and Crowder, 1996). In this example, gamma and short-normal resistivity logs were obtained in a mud-filled borehole in an area of suspected salt-water intrusion. The short normal log shows a gradual drift towards lower resistivity with depth that is attributed to a combination of sediment lithology and water salinity. The two effects can be separated by recognizing that the gamma log is influenced primarily by lithology. If the resistivity log is reversed so that deflections in short normal and gamma are similar for lithologic effects, the two logs are seen to follow each other

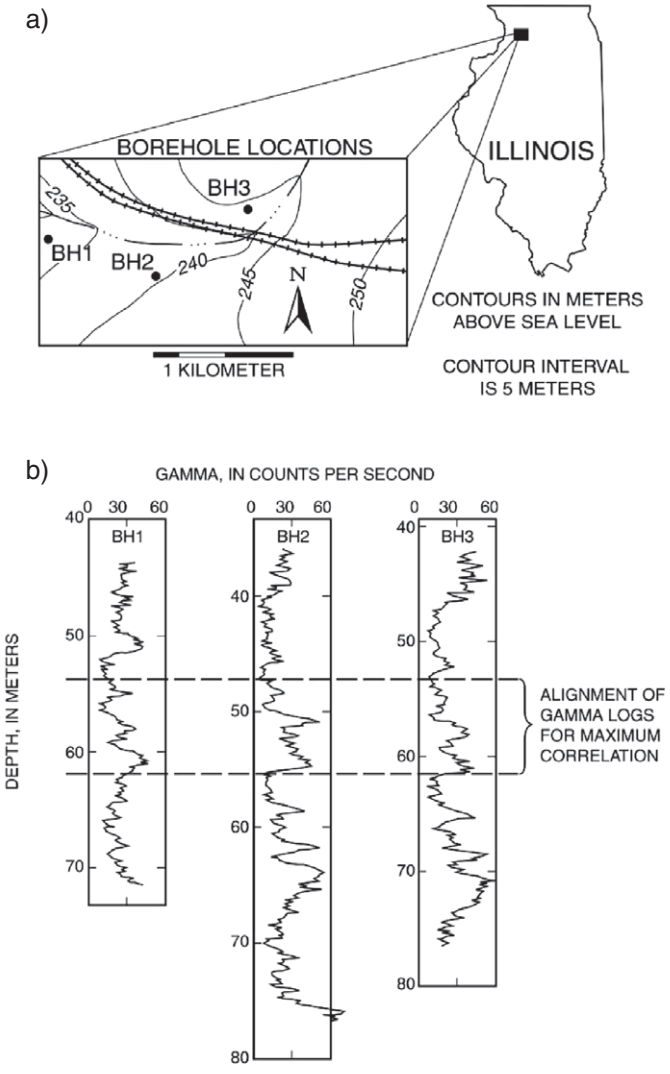

Figure 5. Bed correlation using gamma logs: (a) Location of three boreholes in northwestern Illinois; and (b) alignment of the gamma logs from these boreholes for maximum correlation (Paillet and Crowder, 1996).

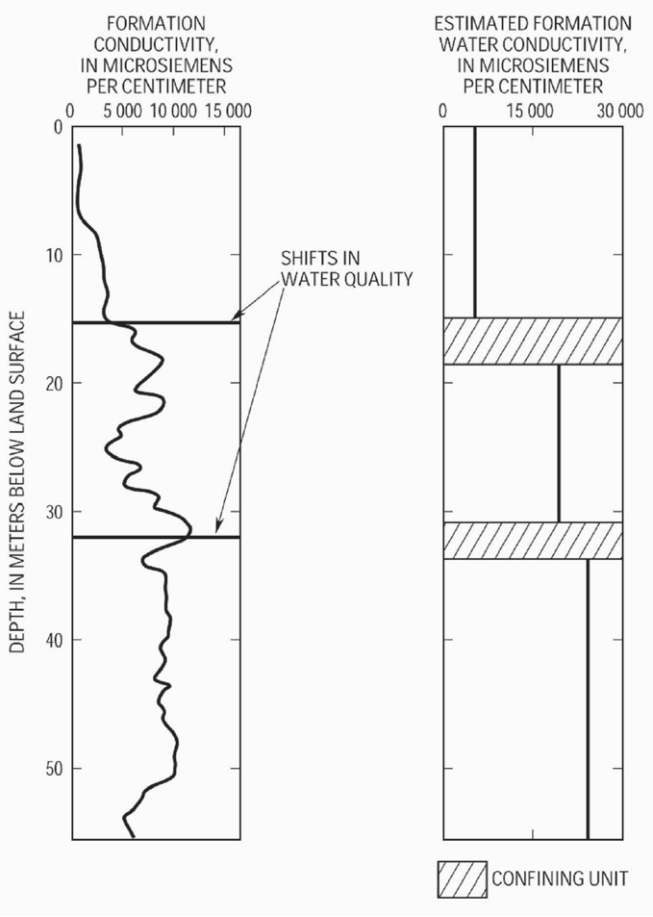

Figure 6. Induction conductivity log from unconsolidated sand and carbonate sediments in south Florida showing the shift information conductivity associated with water quality changes in the aquifer (modified from Paillet and Reese, 2000).

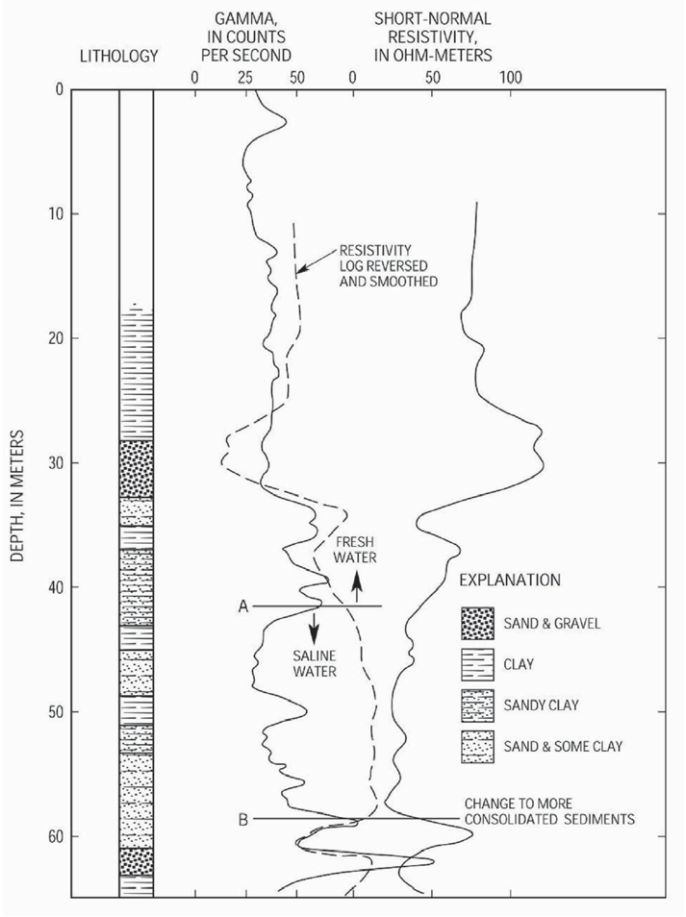

Figure 7. Comparison of gamma and short normal resistivity logs used to indicate the depth of the fresh-water/salt-water interface in alluvial sediments on the coast of Egypt (Paillet and Crowder, 1996).

down to a depth of about 41 m, where they abruptly shift apart. This depth marks the point where a shift in water quality influences the resistivity log but not the gamma log. A deeper shift in the relation between the two logs indicates the contact between the alluvial aquifer sediments and deeper, more consolidated sediments. The logs in Figure 7 illustrate in a qualitative way how multiple logs can be used to uncouple multiple formation parameters in the geophysical interpretation problem. In some applications, qualitative estimations of formation and pore water properties can be made using combinations of geophysical logs; an example is illustrated in Appendix D.

Acoustic log

The seismic properties of the formation (compressional velocity V_P, shear velocity V_S, and sometimes intrinsic attenuation) adjacent to a borehole can be measured with acoustic logging probes (Paillet and Cheng, 1986, 1991). The simplest of these measurements uses a centralized probe to record the time required for an ultrasonic (5 to 40 kHz) signal to travel a certain distance along the borehole wall (Figure 8) (Summers and Broding, 1952). The logging system electronics are designed to pick the first (compressional or P-wave) arrival, and thresholds can sometimes be set to pick the later shear (or S-wave) arrival. Seismic propagation along a fluid-filled borehole is different from seismic propagation at the surface of the earth in a fundamental way. The presence of the fluid column divides the signal into a series of modes related to the resonances of the fluid column (Paillet and White, 1982). The P-waves and S-waves become a series of such waves that can interfere with each other for broad-band source signals. Borehole acoustic-logging probes designed to measure formation V_P (usually given as the inverse or transit time, in microseconds per meter) have to be "tuned" to the proper frequency range to suit borehole diameter and formation properties (Paillet and Cheng, 1991). Slim-logging probes are just now coming into use where the source frequency can be controlled to produce a signal to excite a single P-wave or S-wave mode (Oden et al., 2000). In many situations, the geophysicist will view acoustic logging as the application

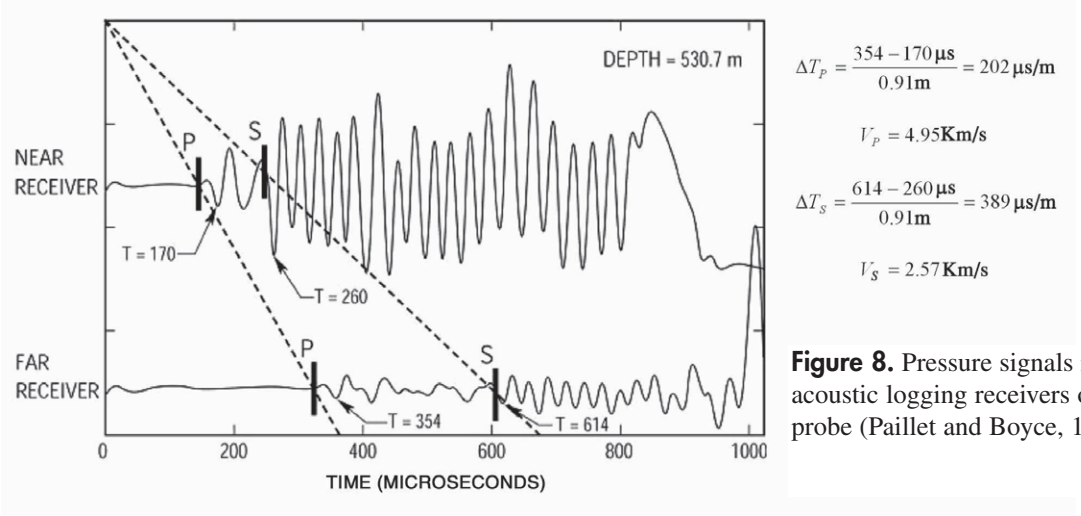

Figure 8. Pressure signals recorded by a pair of acoustic logging receivers on an acoustic logging probe (Paillet and Boyce, 1996).

of a "black box" to generate a profile of formation V_P. In most applications, the acoustic log is plotted in the form of interval transit time (units of μs/m), the inverse of V_p. Acceptable logs are routinely obtained by experienced and qualified operators using the proper equipment, but the log analyst should be aware that there is much more to acoustic logging than just running a "standard" probe using a "standard" configuration. A typical acoustic log interpretation example is presented in Appendix E.

Although acoustic logs are by far the most common form of downhole seismic data obtained by well logging, other seismic properties can be measured by specialized equipment. One form of logging is the full-waveform acoustic log, which records the entire pressure signal at two or more receivers as plotted in Figure 8. In hard rocks, both P-waves and S-waves exist as borehole head-waves and propagate at exactly V_S and V_P (Paillet and Cheng, 1991). In soft formations, where the shear velocity of the formation falls below the acoustic velocity of the borehole fluid, borehole S-waves do not exist. Nonaxisymmetric "shear logging" sources have been designed to generate measurable shear signals in such formations (Kitsunezaki, 1980; White, 1983; Chen, 1989). Although this technique is sometimes advertised as the "direct excitation" of S-waves, the geophysicist knows this cannot be true. Such sources cannot excite S-waves because they apply energy to the borehole fluid, which cannot support shear. These methods work because the nonaxisymmetric sources are simply more effective at exciting wave modes (packets of wave energy) that depend on the shear properties of the formation. However, these are dispersive wave modes and not a true S-wave. They propagate at a group velocity somewhat less than true V_S (Figure 9; Paillet and Boyce, 1996). The example shows a conventional axisymmetric logging signal compared to the signal from a nonaxisymmetric shear logging source for a basalt formation, where true P-waves and S-waves can propagate. The conventional source shows P-wave and S-wave arrivals. The shear logging source shows the same P-wave arrival with much reduced amplitude, but the dispersive shear mode lags somewhat behind the true S-wave. This does not mean that such shear logging does not work, only that sophisticated mode inversion methods are needed to make estimates of formation V_S using the spectral dispersion of the recorded waves. Furthermore, this method can be used for "soft" rocks or "slow" formations where S-waves cannot propagate along boreholes (Paillet and Cheng, 1991; Paillet et al., 1992).

Borehole image log

Specialized borehole image logs are obtained using optical (Williams and Johnson, 2000), acoustic (Zemanek et al., 1970), or electrical imaging methods (Ekstrom et al.,

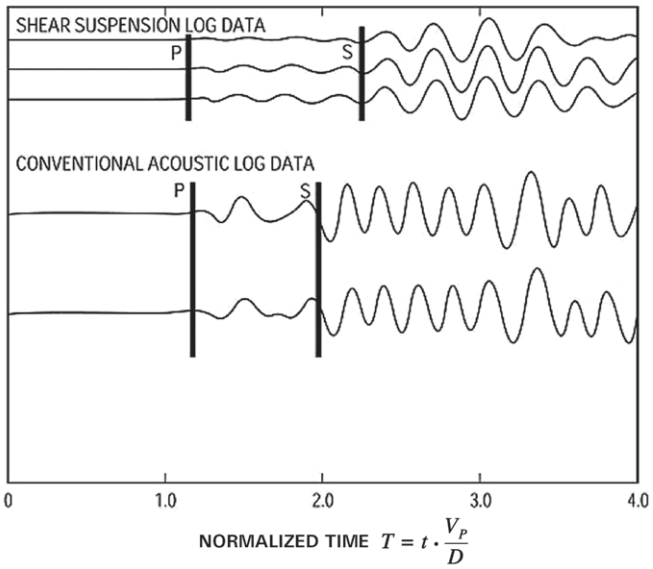

Figure 9. Comparison of acoustic waveforms from receivers on a conventional axisymmetric acoustic logging probe with those from an axisymmetric shear logging probe, where data were obtained from the same interval in a massive basalt formation (Paillet and Boyce, 1996).

1987). A typical example is illustrated in Figure 10, showing the pattern of acoustic reflectivity generated by scanning the borehole wall with an ultrasonic (500 kHz to 1.25 MHz) pulsed source (acoustic televiewer). This technique is useful for casing inspection, fracture characterization, and locating bed boundaries (Long et al., 1996). Optical scanning devices give color images for lithology identification and provide better spatial resolution, but are limited to operation in clear fluids or air-filled boreholes. Black-and-white reproductions of optical image logs in typical formations cannot illustrate the use of color images to identify lithology, but do indicate the greater spatial resolution of optical images compared to acoustic images, and the ability to detect veins and mineralized fractures that are not indicated by acoustic images (Figure 11). One of the main limitations on borehole imaging devices is the lack of borehole wall penetration. Image data apply to the highly local conditions at the borehole wall, and represent the formation as affected by drilling damage and contact with borehole fluids. For example, local measurements of fracture strike, dip, and aperture may not be indicative of fracture or fault properties over larger and more representative sections of the same subsurface feature. However, the fine-scale detail of borehole image logs can be integrated with other log data to provide an enhanced interpretation of formation properties (Figure 12; Paillet, 2000). Such composite logs combine the borehole wall images of bed contacts and fractures with the measured effect on the volume-averaged properties of the formation containing those features.

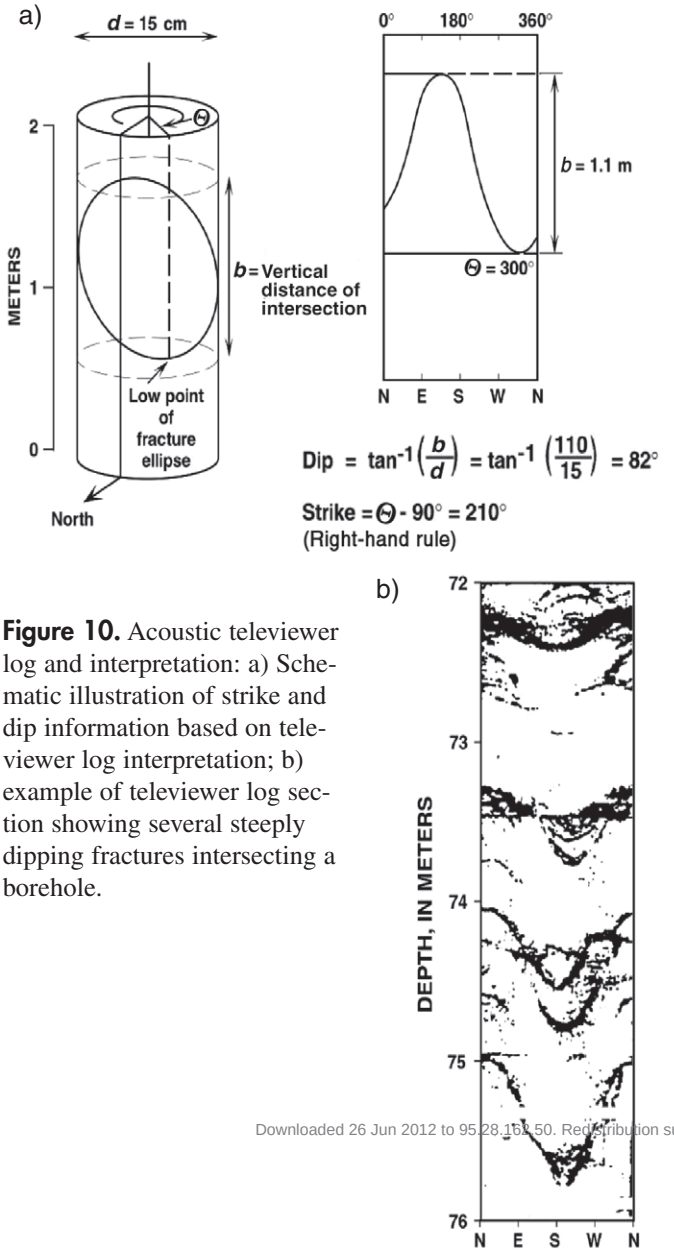

Figure 10. Acoustic televiewer log and interpretation: a) Schematic illustration of strike and dip information based on televiewer log interpretation; b) example of televiewer log section showing several steeply dipping fractures intersecting a borehole.

Borehole flow log

Some of the most important applications of near-surface geophysical logging are in hydrogeology. Most logs provide geophysical measurements that are interpreted to give indirect estimates of hydraulic properties of sediments. Borehole flow logs are an exception in that they provide direct measurements of the hydraulic properties of the formations adjacent to boreholes. New, high-resolution flow logging techniques (Hess, 1986; Molz et al., 1994) make it relatively simple to measure flow in boreholes under ambient, pumping, or injection conditions (Figure 12). In this example, upflow is positive and downflow defined as negative, so that inflow to the borehole can be given as the difference of flow above and below each inflow point. Because inflow to the borehole is driven by the product of permeability (expressed as relative interval transmissivity) and pressure gradient, two different flow profiles (in this case, ambient and steady injection) are required to give estimates for each of these parameters at each inflow point. These logs can be used to generate estimates of the hydraulic conductivity of water-producing intervals in boreholes, given in units of hydraulic transmissivity (m^2/s). As in the case of borehole image logs, flow logs are even more useful when combined with other log data. These combinations can be used to identify the nature of water-producing zones, and to fit the "plumbing" indicated by those zones into the large-scale geologic structure. An example is illustrated in Figure 13, where stratigraphic data from the gamma log, producing-zone character from the televiewer log, and the identity of water-producing zones from the flow log are used to show how permeable bedding-plane openings are fit into the regional stratigraphic column. The addition of flow logs to the log suite adds an entirely new dimension to geophysical log interpretation for groundwater applications.

Direct-Push Methods

Direct-push technology is a scaled-down version of drilling, sampling, and logging where rigid rods are pushed into unconsolidated sediments (Endres and Clement,

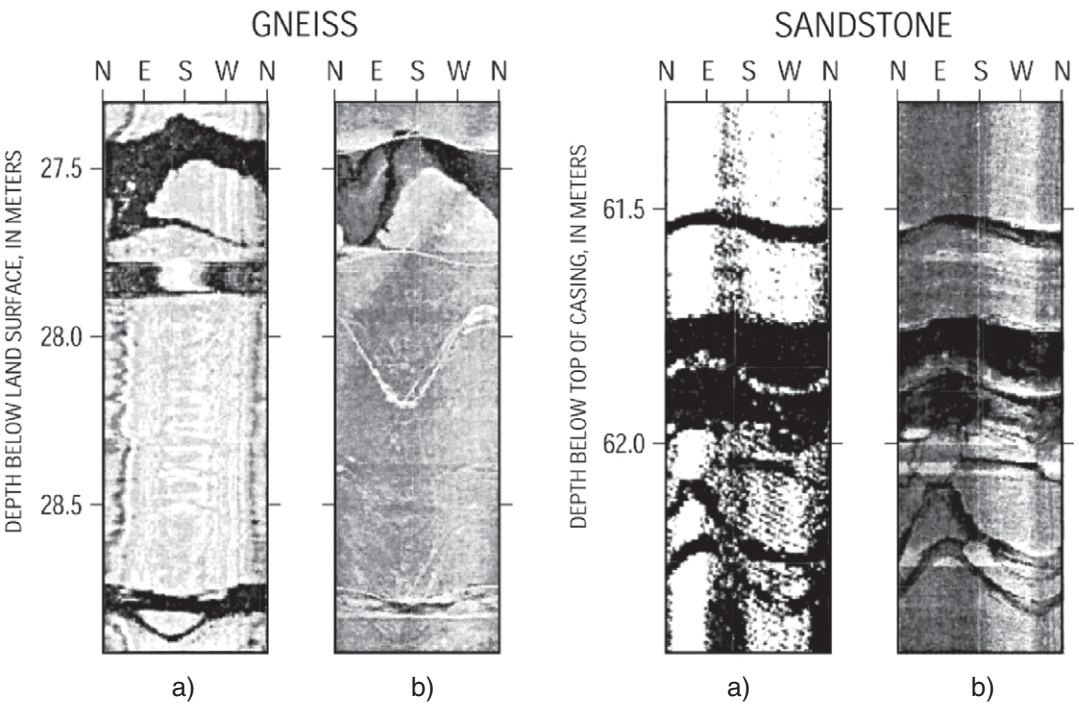

Figure 11. Comparison of (a) acoustic and (b) optical borehole image logs in a 75-mm-diameter borehole for metamorphic and for sandstone lithology (Williams and Johnson, 2000).

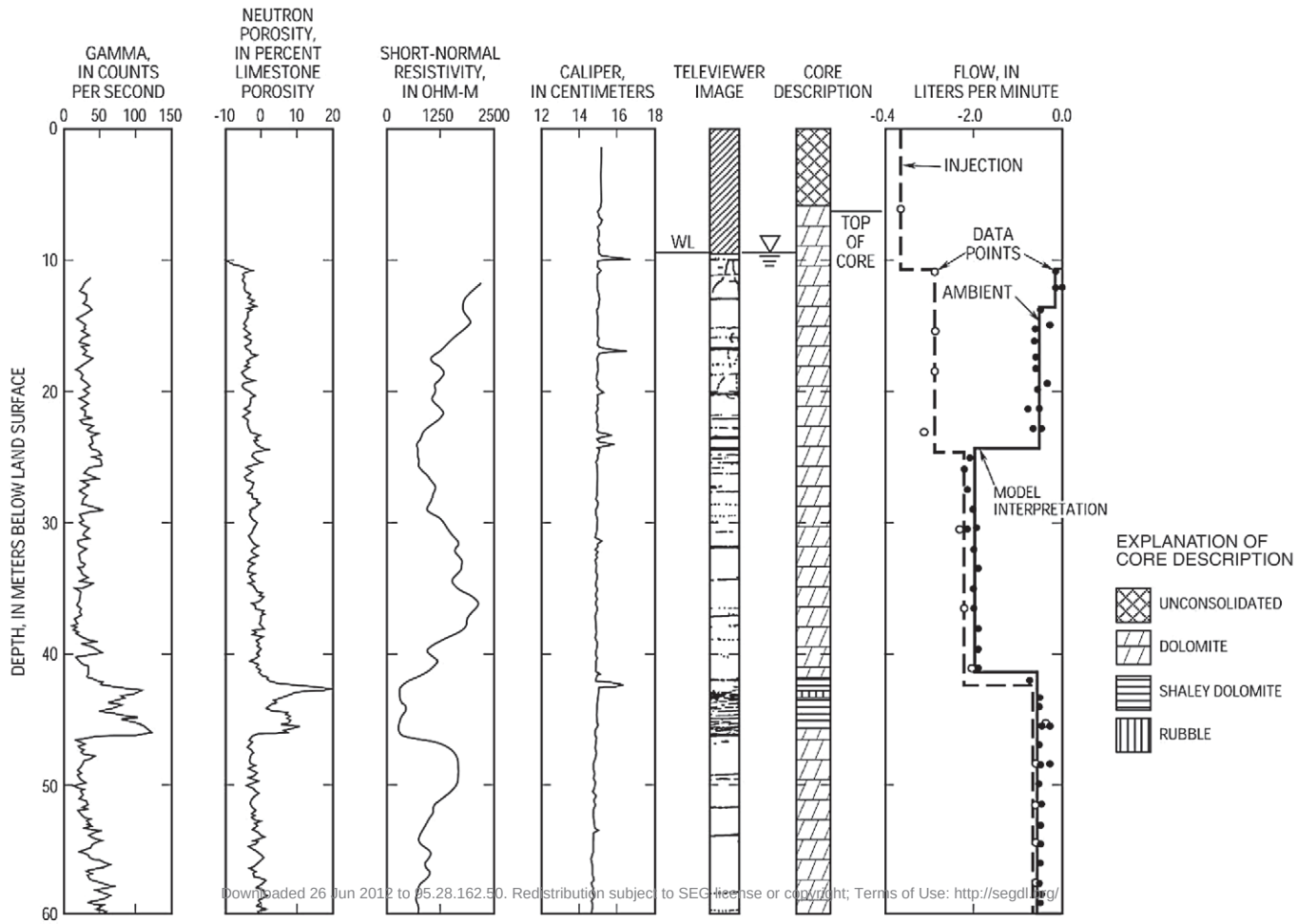

Figure 12. Composite of geophysical logs, televiewer borehole wall image, core description, and borehole flowmeter profiles from a borehole in central Wisconsin (Paillet, 2000).

1998). These methods are ideally suited for shallow subsurface investigation (depths limited to at most 50 m) in environmental studies where the release of contaminants by conventional drilling would be unacceptable. Direct-push equipment generally is smaller and lighter than most conventional drilling equipment, so that site access is improved, and numerous subsurface samplings can be made in a confined area. Measurements are made with minimal disruption to the geologic environment and do not require a pre-existing borehole; fluids and gases can be sampled from a precisely defined depth (McCall and Zimmerman, 2000). Push rods provide access for fiber optic cable technology such as laser florescence used to identify organic contaminants in situ. Direct-push equipment readily provides for grout injection when push rods are withdrawn. Thus, direct-push methods were developed to suit the needs of environmental studies of the shallow subsurface where conventional drilling and sampling would not be very effective, and would have unacceptable environmental consequences.

For the purposes of this review, direct-push methods are considered analogous to conventional geophysical logging, except that geophysical sensors are inserted by means of push rods instead of wireline and winch (Figure 14). Geophysical sensors, such as the electrical conductivity probe shown in Figure 14, can be attached to the tip of the push rods to provide a profile of physical properties as the rods are inserted into the subsurface (Figure 15) (Milsom, 1989). Direct-push logs also provide a record of the rate of penetration of the rods, providing a separate and unique log that can be related to sediment properties (Mitchell and Brandon, 1998; Robertson and Campanella, 1983). One distinct advantage is that push-technology logs do not contain a "blind" interval immediately below the surface where surface casing and grout generally invalidate conventional geophysical logs in most boreholes. Another advantage is that the sensor is completely surrounded by the formation so there is no influence of water-filled annulus or casing on the subsurface measurement. Otherwise, the direct-push logs can be analyzed with all of the techniques used in geophysical well log analysis, such as the construction of sections based on the correlation of beds across borehole profiles (Figure 16).

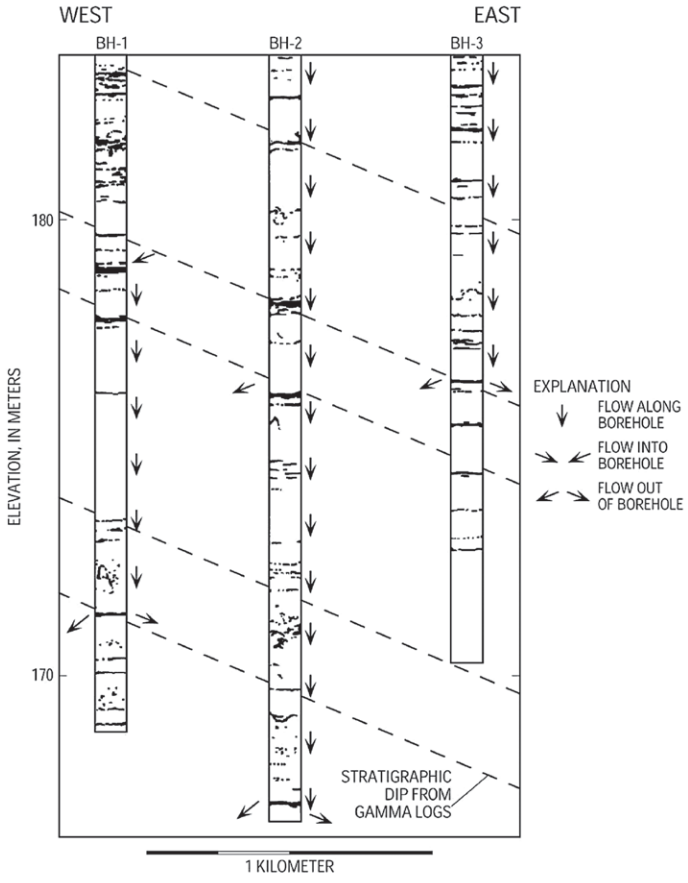

Figure 13. Televiewer logs from three different boreholes aligned along the regional stratigraphic dip and showing water-producing bedding planes identified from flowmeter profiles under ambient hydraulic-head conditions; compare to data in Figure 17 (Paillet and Crowder, 1996).

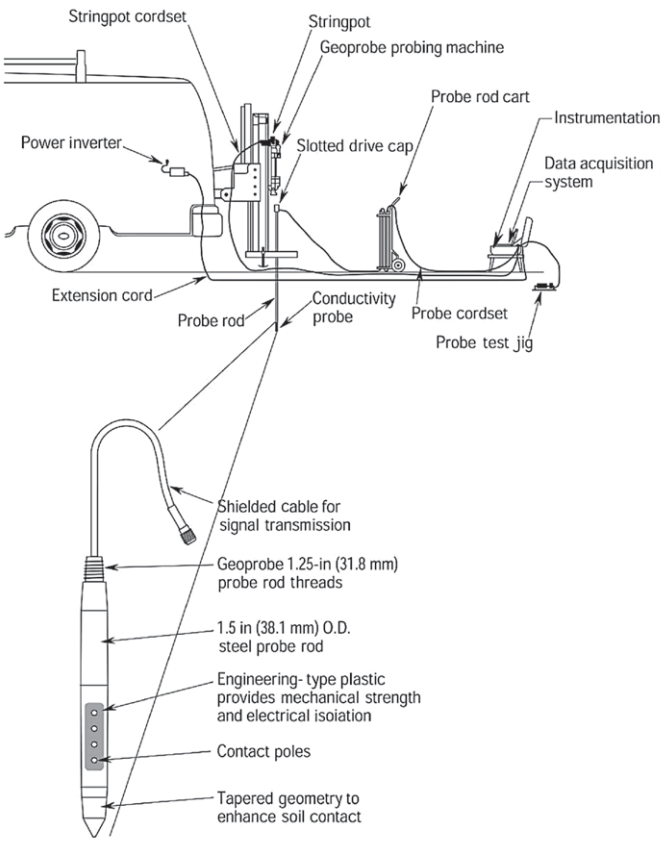

Figure 14. Schematic illustration of direct-push drilling equipment, showing the details of a subsurface conductivity probe attached to the tip of the push rod (from McCall and Zimmerman, 2000).

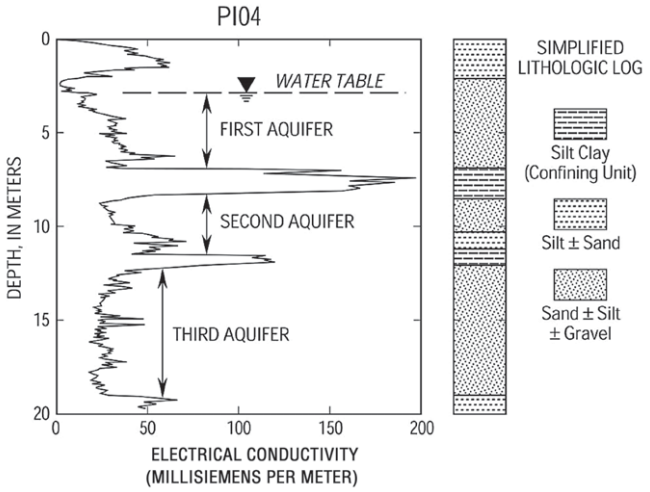

Figure 15. Typical formation conductivity log compared to recorded rate of rod penetration and interpreted lithology for the equipment illustrated in Figure 14 (from McCall and Zimmerman, 2000).

Hydrophysical Logging

Hydrophysical logging is a highly specialized logging technique designed to estimate the permeability of water producing zones intersecting boreholes, while simultaneously yielding an estimate of the electrical conductivity of the water entering at each zone. The technique is based on the introduction of deionized water into a borehole and then repeated fluid column electrical conductivity logging as electrically conductive water flows into the borehole (Tsang et al., 1990). "Time lapse" presentations of the fluid column logs illustrate where formation water enters the borehole and is convected up, down, or across the borehole under the flow regime (Figure 17). Quantitative estimates of zone transmissivity (the product of zone permeability and thickness) and the electrical conductivity of the water in the zone are made by analyzing the evolution of the borehole fluid conductivity over time (Tsang et al., 1990; Paillet and Pedler, 1996; Paillet et al., 1993). Fluid column and borehole flow modeling is possible when the fluid column displacement and subsequent evolution of the borehole flow field are designed so as to satisfy an initial boundary value problem that can be fit to a numerical solution.

In the simplest situation, deionized water is pumped into the lower part of a borehole while water is pumped from the top of the fluid column so as to replace the fluid column with minimum hydraulic disturbance. Then, the inflow of formation water after the sudden onset of pumping can be modeled as an initial value problem (Figure 17a). In situations where there is flow between zones under ambient conditions, the hydrophysical logging is performed under both ambient and steady pumping conditions (Figure 17b). In this example, ambient flow is downward, so that the electrical conductivity signal of the lowermost

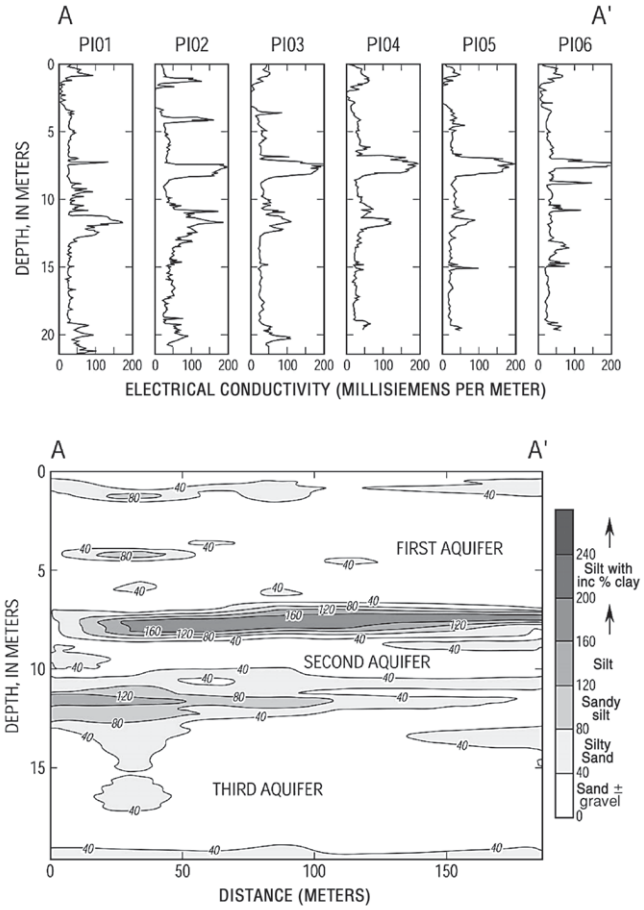

Figure 16. Formation conductivity profiles in a cross-section used to interpret subsurface aquifer structure (from McCall and Zimmerman, 2000).

zone accepting water under ambient conditions cannot be determined from the fluid column logs. The electrical conductivity of water from this zone is indicated when upflow is induced by pumping, and the difference in the amount of zone inflow can be used to correct zone transmissivity estimates for the presence of a vertical hydraulic-head gradient. In general, the hydrophysical logging technique provides more accurate estimates of zone transmissivity over a greater range of values than can be obtained with borehole flow logging, but the technique has the disadvantage of requiring equipment for handling and emplacing borehole fluids.

Borehole Radar

Ground-penetrating radar (GPR) measurements can be made in boreholes in a way virtually identical to other forms of well logging, using essentially the same equipment as used in GPR surveys at the ground surface. The downhole use of this technique is especially effective because borehole use avoids the attenuating effects of surficial weathered zones that commonly affect surface radar

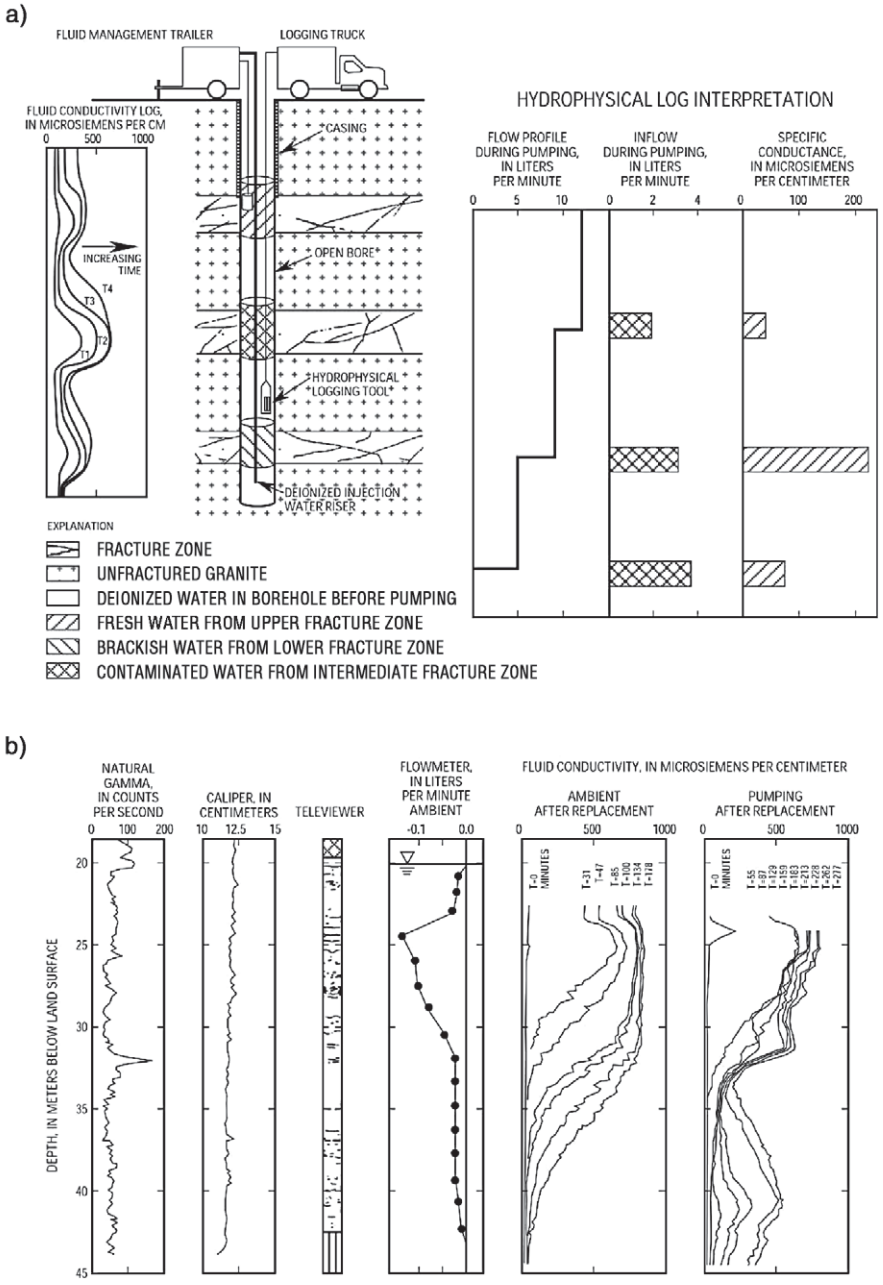

Figure 17. (a) Schematic illustration of the application of hydrophysical logging in a borehole under steady pumping, showing logs interpreted in terms of relative zone inflow and formation fluid electrical conductivity (from Paillet and Pedler, 1996); and (b) hydrophysical logs from a borehole with ambient flow under both ambient and steady pumping conditions (from Paillet et al., 1993).

profiles (Olsson et al., 1992; Lane et al., 1998b). Borehole radar logs generally are treated separately from other logs for several important reasons: (1) the scale of investigation is substantially greater than that of other logs, (2) the measurements can be assigned an orientation by controlling source and receiver function, and (3) interpretation techniques are similar to those used in seismic-reflection processing and are very different from other log-analysis techniques. One of the most common applications of borehole radar is in the detection of faults, fractures, and lithologic contacts located at distances up to 100 m from boreholes in crystalline or consolidated sedimentary rocks. In a typical example (Figure 18; Stumm et al., 2000), radar indicates a major fracture or fault zone approximately 30 m from a borehole. The steeply dipping orientation of the feature indicates that it does not intersect the borehole. However, the radar reflector in Figure 18 corresponded to a hydraulically conductive fracture zone intersecting an aqueduct tunnel subsequently constructed at this location.

Borehole-to-Borehole Methods

Introductory remarks

This section of the chapter introduces borehole-to-borehole radar and borehole-to-borehole seismic methods. The discussion is limited to these two techniques because they are the most frequently used and are similar in concept. The section focuses on procedures that are currently used to collect, process, and interpret borehole-to-borehole data. The section does not discuss advanced procedures that are still research topics; these advanced procedures include diffraction tomography (Tura et al., 1992), full waveform inversion (Reiter and Rodi, 1996; Zhou et al., 1997), and inclusion of hydrogeological data during an inversion (Hyndman and Harris, 1996; Hubbard et al., 1999). Also, the section does not discuss borehole-to-borehole electrical resistivity (Daily et al., 1995; LaBrecque et al., 1996; Ramirez et al., 1996) and borehole-to-borehole S-wave measurements (Sirles and Viksne, 1990) because these two methods are used relatively infrequently.

Figure 1d illustrates data collection for a borehole-to-borehole radar survey. The left borehole contains the transmitting antenna, and the right borehole contains the receiving antenna. As the radar waves propagate between the antennas, they are affected by heterogeneity in the electro-

magnetic properties, like the dielectric permittivity. Afterwards, the radar data are processed to map the heterogeneities in the (approximately) planar region between the wells. The estimated properties of the heterogeneities are then interpreted in terms of the geology or the hydrogeology; for example, high dielectric permittivity might indicate the presence of water. This process illustrates the essence of a borehole-to-borehole geophysical survey.

This section is divided into eight subsections. The next two subsections discuss the propagation of radar and seismic waves between boreholes; understanding propagation is crucial to understanding the techniques. The next three subsections discuss data collection, data processing, and data interpretation. The discussion of data processing includes some pitfalls, and the discussion of data interpretation is based on field data. The last two subsections contain references to case histories and to public-domain software for data analysis.

To make this section clear, it is necessary to define some terms. The term *borehole-to-borehole radar* is used because it more precisely describes the technique than the common term *crosswell radar* does. For the same reason, the term *borehole-to-borehole seismic* is used. *Source* refers to either the transmitting antenna or the seismic source, and *receiver* refers to either the receiving antenna or the seismic receiver. Thus, *source borehole* refers to the borehole with either the transmitting antenna or the seismic source, and *source location* refers to the spatial location of either the transmitting antenna or the seismic source.

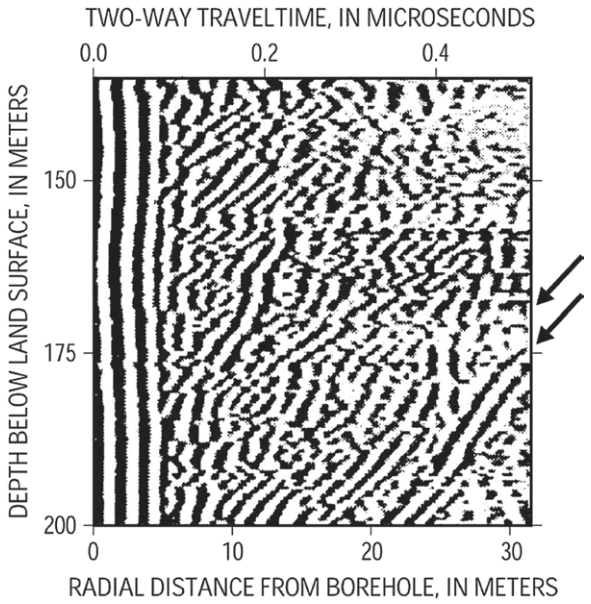

Figure 18. Example of directional borehole radar data used to identify a steeply dipping reflector located about 30 m away from a borehole in gneiss bedrock (Stumm et al., 2000).

Radar wave propagation between boreholes

For borehole-to-borehole radar, the transmitting antenna is commonly a linear dipole that is loaded with resistors to suppress ringing (Figure 19a and b). The dipole mostly generates a transverse-magnetic wave (Figure 19c). Part of the radar wave radiates into the formation, and another part

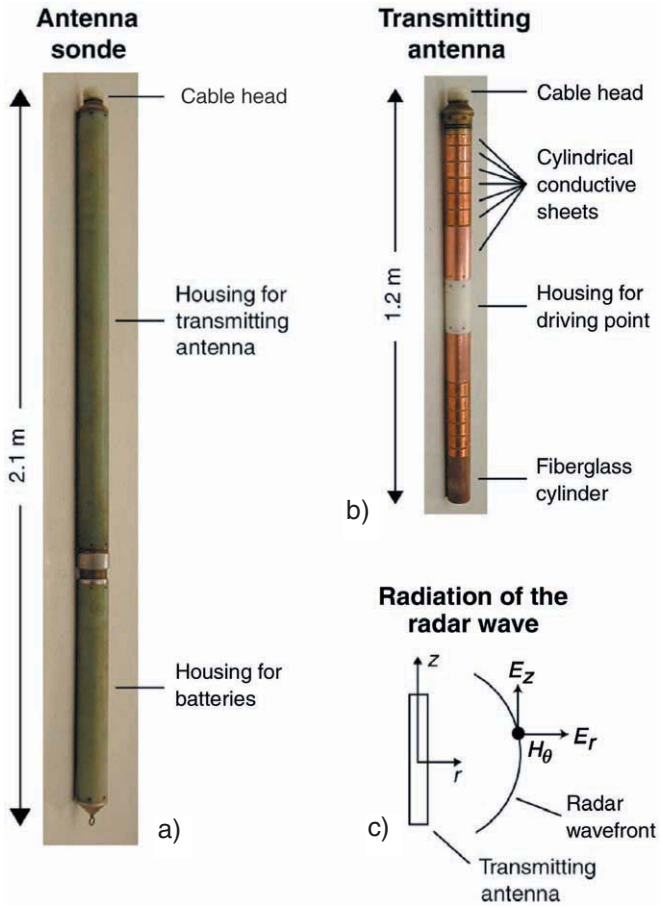

Figure 19. (a) Sonde for a transmitting (radar) antenna. The cable head connects to a fiber-optic cable along which signals are sent to the sonde. The batteries power the antenna. (b) Transmitting antenna. The conductive, cylindrical sheets are mounted on the fiberglass cylinder and are connected to each other with resistors. The conductive sheets are also connected to the driving point (not shown). A voltage pulse is applied at the driving point; the associated currents propagate along the conductive sheets and radiate the electromagnetic (radar) waves. (c) Radiation of the transverse magnetic radar wave. In the cylindrical coordinate system aligned with the antenna, the radar wave has components of the electric field intensity in the radial and the axial directions (E_r and E_z). The radar wave also has a component of the magnetic field intensity in the azimuthal direction (H_θ), which is perpendicular to the plane of the figure. (Photographs courtesy of D. L. Wright, U. S. Geological Survey.)

propagates along the borehole as a guided wave (Wright et al., 1984; Bradley and Wright, 1987; and Dubois, 1995). The radiation of the radar wave into the formation has been analyzed theoretically by King et al. (1981, p. 489-526) and by Holliger and Bergmann (2000). The guided wave has been analyzed theoretically by Ebihara et al. (1998).

As the radar wave propagates through the formation, it is reflected, refracted, and diffracted by heterogeneity in the electromagnetic properties. The radar wave eventually passes the borehole with the receiving antenna, and some of its energy is transmitted into this borehole and is detected by the receiving antenna. The receiving antenna is usually a linear dipole loaded with resistors. The voltage from the antenna is transmitted along a coaxial cable to electronic equipment on the ground surface, which digitizes and records the voltage; alternatively, the voltage is digitized by electronic equipment housed within the antenna sonde, and then the digitized signal is sent along a fiber optic cable to the surface where it is recorded. Also, some of the energy transmitted into the borehole can propagate along the borehole as a guided wave; this guided wave is detected by the receiving antenna and consequently affects the radar trace (Sato and Thierbach, 1991).

An example of borehole-to-borehole radar data is shown in Figure 20. The spacing between the boreholes was about 24 m; the bedrock consisted of schist, granite, and pegmatite. Both antennas were linear dipoles, similar to that shown in Figure 19. Each recorded trace consists of 512 stacked traces—the stacking reduced random noise. The prominent event in the traces corresponds to the radar wave.

Seismic wave propagation between boreholes

For borehole-to-borehole seismic surveys, the source usually generates a P-wave in the borehole fluid. This might be done, for example, with an electrical spark or a piezoelectric transducer (Figure 21a). The P-wave propagates from the source to the borehole wall where some of its energy is transmitted into the formation as P- and S-waves. The remaining energy is reflected back from the borehole wall. This reflected wave generates a guided wave that propagates along the borehole; the guided wave is commonly called either a *tube wave* or a *Stoneley wave*. A summary of field studies regarding waves in boreholes is given by White (1983, 140–145); the radiation of the P-

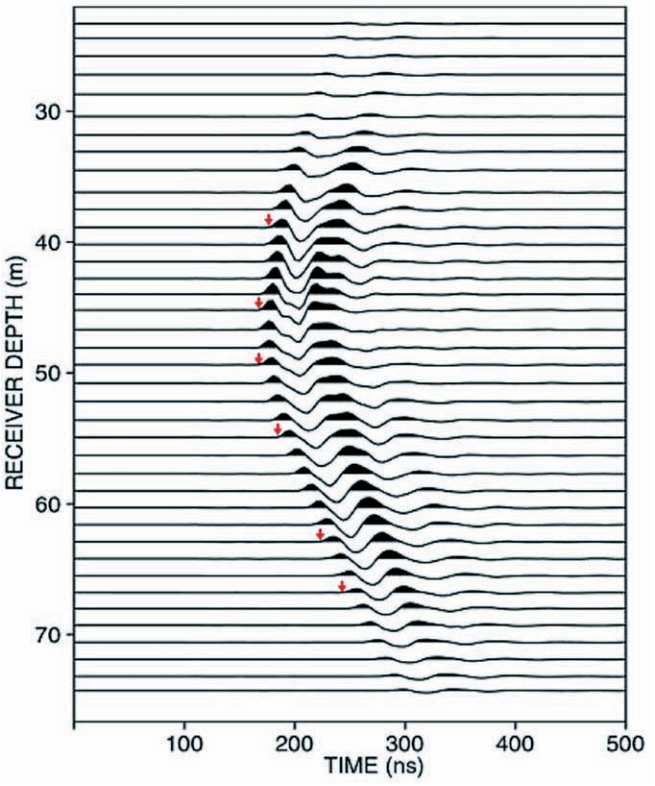

Figure 20. An example of borehole-to-borehole radar data. The transmitting antenna was fixed at about 42 m depth, and the receiving antenna was moved up the receiver borehole. The arrows indicate, for a few traces, where the traveltime of the radar wave would be picked. (Data courtesy of D. L. Wright and J. Abraham, U. S. Geological Survey).

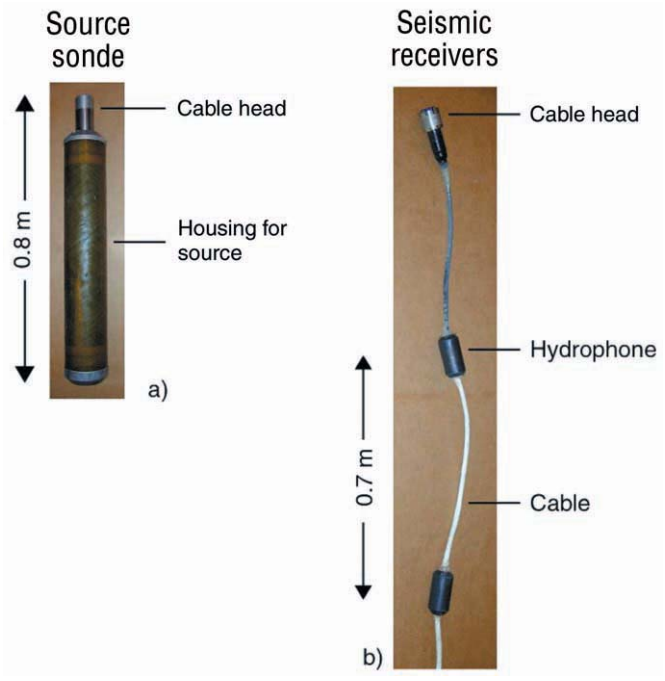

Figure 21. (a) Sonde for a seismic source. The source consists of about 220 piezoelectric transducers; to fire the source, the transducers are excited simultaneously (Wong, 2000). The sonde is filled with oil so that P-waves readily propagate from the transducers, through the housing, and into the borehole fluid. (b) Top of an array of seismic receivers. Each receiver is a piezoelectric transducer; this type of receiver is often called a hydrophone. (Photographs courtesy of L. V. Block, U. S. Bureau of Reclamation.)

and the S-waves into the formation has been analyzed theoretically by Lee and Balch (1982), Meridith (1990), and Gibson (1994). Some sources, that clamp to the borehole wall, are used to generate S-waves for measurements of S-wave velocity; see Sirles and Viksne (1990).

As the P- and S-waves propagate through the formation, they are reflected, refracted, and diffracted by heterogeneity in both the elastic properties and the density. Both waves eventually propagate past the borehole with the receiver array, and some of their energy is transmitted into the borehole as P-waves, which are detected by an array of receivers. Usually the receivers are piezoelectric pressure transducers (Figure 21b), which detect pressure fluctuations. The transducers generate a voltage that is transmitted to the ground surface where the voltage is digitized and then recorded by a seismograph. The reception of the P- and the S-waves has been analyzed theoretically by Peng et al. (1993, 1994).

Sometimes, the propagation of the seismic waves is more complex than was previously described. Under certain conditions, the tube wave in the source borehole radiates S-waves into the formation (Meredith et al., 1993). When the tube wave hits the bottom of the borehole or the air-water interface in the borehole, the tube wave radiates seismic waves into the formation. When collecting data in fractured bedrock, the tube wave in the source borehole injects water into open fractures intersecting the source borehole, and these fractures act as secondary sources. In addition, as the P-wave passes the receiver borehole, it compresses (and dilates) the fractures, injecting water into the receiving borehole; this disturbance propagates along the receiving borehole as a tube wave, a phenomenon that has also been observed in surface-to-borehole seismic data (Beydoun et al., 1985; Hardin et al., 1987; Cicerone, 1991).

An example of borehole-to-borehole seismic data is shown in Figure 22. The spacing between the boreholes was about 26 m; the bedrock consisted of schist, granite, and pegmatite. The source was a piezoelectric transducer that was excited by a pulse of about 5 to 10 kV. The source was fired about 50 times, and the traces from each firing were stacked to reduce the random noise. The large amplitude event corresponds to the P-wave in the formation; an event corresponding to the S-wave is not identified in these traces.

Data collection

Figure 23 shows one example of how borehole-to-borehole radar data might be collected. The source is near the bottom of the source borehole, and the receiver is near the bottom of the receiver borehole (Figure 23a). A radar trace is recorded for this configuration. For the next and each of the subsequent configurations, the receiver is moved up (Figure 23b), and a radar trace is recorded. This procedure continues until either the receiver is at the top of the borehole or the radar wave cannot be observed in the traces. Then, the receiver is returned to the bottom of the receiver borehole, and the source is moved up (Figure 23c). This procedure is repeated until the source is at the top of the source borehole. With this method of collecting data, the region between the two boreholes is probed in many different directions (Figure 23d)—a direction is defined by the ray between the source and a receiver. The thoroughness of probing is also affected by the distances between the source locations along the source borehole; likewise, it is affected by the distances between the receiver locations along the receiver borehole.

The collection of borehole-to-borehole seismic data is generally similar; the most significant difference is that seismic traces from many depths can be recorded simultaneously using an array of receivers.

The source and receiver locations must be known to process borehole-to-borehole data. Typically, the calcula-

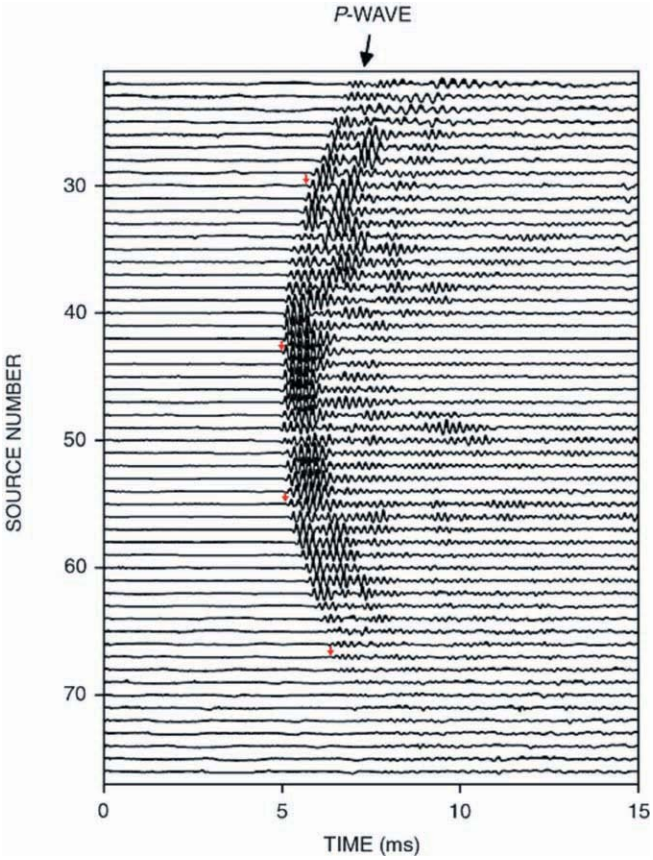

Figure 22. An example of borehole-to-borehole seismic data. These seismograms were recorded by one receiver, which was at 46 m depth. The depth of the source, in meters, roughly equals the source number. The arrows indicate, for a few traces, where the traveltime of the P-wave would be picked.

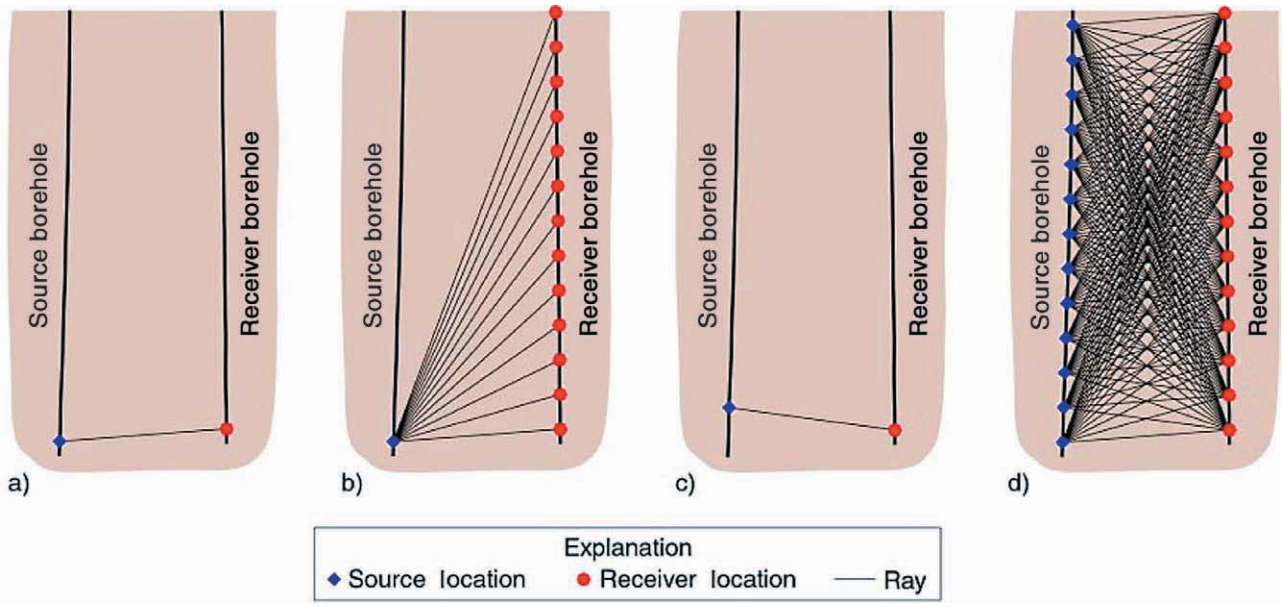

Figure 23. A typical procedure used to collect borehole-to-borehole radar data.

tion of the locations requires three different sets of measurements. The first set comprises the cable depths of the source and the receivers within the boreholes. The cable depth of the source, for example, is the distance along the cable between the source and some reference, which is usually the top of the casing. The second set comprises the deviations of the boreholes, which are measured with a borehole deviation tool and are typically referenced to the tops of the casings. (Borehole deviation may be merely 1 or 2 m, but this distance is often significant compared to both the wavelength and the distance between the boreholes.) The last set of measurements is the locations of the tops of the casings, which are determined with a survey.

Data processing

The goal of the processing is to extract information from the radar and the seismic traces and then use that information to estimate formation properties. Because both radar- and seismic-wave propagation is complex, the traces contain a lot of information. Typically, the processing focuses on the simplest information in the traces: the traveltime of either the radar wave or the seismic P-wave.

One way to pick traveltimes is to sort the traces into groups, which are called *gathers*. (For borehole-to-borehole seismic data, a particularly useful gather consists of all traces for one receiver location. The advantage of this gather is that the effects of mismatched receivers are not apparent in the gather, making picking easier.) The traces from a gather are displayed on a computer screen, where the traces can be readily scaled to see fine details, filtered to remove noise, and shifted to visually correlate adjacent traces. The pick is made at the first arrival of the radar wave (Figure 20) or P-wave (Figure 22).

Although picking traveltimes appears to be simple, it is usually difficult. One reason for the difficulty is that the amplitude of the radar wave or the P-wave may be low compared to the noise on the trace. Low amplitudes occur, for example, when the source is much higher than the receiver (or vice versa) or when a radar wave propagates through a region with high electrical conductivity like clay. A second reason is that the onset of the radar wave or the P-wave may be gradual instead of sharp and well defined. Another reason is that the character of the radar wave or the P-wave may change abruptly, making correlation of adjacent traces poor. For example, such changes may occur in seismic data near fractures intersecting the source or the receiver borehole. Because of the difficulties in picking traveltimes, checking them is important, and this may be done using various different plots of the traveltimes (Majer et al., 1990; Pratt et al., 1993).

To estimate the radar or P-wave velocity in the formation, their traveltimes must be calculated. The traveltimes are rarely calculated with the electromagnetic or elastic wave equations, because the calculations require too much time and computer memory. Instead, the calculations are usually made with approximations to the wave equations. For both electromagnetic and elastic wave propagation, the approximate equations are identical and both are called the *eikonal equation*:

$$(\nabla T)^2 = \frac{1}{c^2}, \tag{5}$$

where ∇ is the gradient, T is the traveltime on the wavefront, and c is the phase velocity of either the radar wave or the P-wave (Born and Wolf, 1989, 110–112; Aki and Richards, 1980, 89–90). The eikonal equation is often solved using ray tracing.

Because both borehole-to-borehole radar and borehole-to-borehole seismic use the eikonal equation, the same inversion algorithm can be used to estimate the radar or the P-wave velocities. For an inversion, the formation must be represented by a mathematical model. A commonly used model consists of a two-dimensional plane that passes through both boreholes. The plane is divided into many rectangular cells, and in each cell the velocity (or its reciprocal, slowness) is isotropic and constant. Using the velocities within the cells, the inversion calculates the traveltime between each source and each receiver. Based on the difference between the calculated and the measured traveltimes, the inversion changes the velocities in the cells. This procedure is repeated until the calculated and the measured traveltimes are satisfactorily matched—the criterion for the match must be specified by the geophysicist.

There are several inversion algorithms. For the first borehole-to-borehole investigations, geophysicists usually used two algorithms adopted from medical tomography: the algebraic reconstruction technique (ART) and the simultaneous iterative reconstruction technique (SIRT) (Lytle and Dines, 1980; Peterson et al., 1985; Lo and Inderwiesen, 1994, 43–50). Recently, some geophysicists have switched to inversions based on matrix methods, which use the conjugate gradient method to invert matrices (Scales, 1987). A particular implementation of these matrix methods, which is called algorithm LSQR (Paige and Saunders, 1982), converges much faster to a final solution than SIRT does (Nolet, 1985). An additional advantage of the matrix methods is that they can be used to assess the quality of the inversion; this assessment is done with the model covariance matrix, which shows how errors in the traveltimes affect the estimated velocities, and with the resolution matrix, which shows how well the velocity in each cell can be uniquely determined (Aki and Richards, 1980, 687–689; Vasco et al., 1998).

As the data are being processed, several difficulties might arise. If the boreholes deviate outside the two-dimensional planar model used for the inversion, the source and the receiver locations will have to be projected into the model. If the deviation is large (compared to the interborehole distance), then the projection will cause a significant change in the distance between the sources and the receivers. Such changes introduce large anomalies into the tomogram (Maurer, 1996). A way to overcome this problem is to use a three-dimensional model to accurately locate the sources and the receivers in three dimensions. Within the inversion, the velocities are kept constant in the direction perpendicular to the plane passing approximately through the two boreholes. In other words, the velocities may vary in two dimensions, although the model itself is three dimensional.

Another difficulty is anisotropy. The causes of anisotropy in seismic waves are reviewed by Crampin et al. (1984) and Crampin (1987). The causes of anisotropy in radar waves are just beginning to be studied; some field data indicate that one cause is the alignment of minerals in rocks (Tillard, 1994). The velocity anisotropy may be manifested as a systematic pattern in various plots of the traveltimes (Majer et al., 1990, 59; Vasco et al., 1997) and in the traveltime residuals from an inversion using isotropic velocities (Pratt et al., 1993; Williamson, 1993). Several processing methods can account for anisotropy. In one method, the anisotropy is measured or estimated independently of the borehole-to-borehole data. Based on these measurements, the traveltimes are adjusted, and the adjusted traveltimes are used in an isotropic inversion (Majer et al., 1990, 71–73). In a method appropriate for sedimentary rocks, the anisotropy is measured or estimated for the anisotropic layer; the depth coordinates for that layer are stretched; an isotropic inversion is applied; and finally, the depth stretch is removed (Saito, 1991). In a method that is appropriate for weakly anisotropic rock, the elastic constants are estimated by separating them into an isotropic part and an anisotropic part (Chapman and Pratt, 1992; Pratt and Chapman, 1992; Vasco et al., 1997). Although this method is general, the anisotropic part is difficult to resolve (Vasco et al., 1998; Williamson, 1998).

In addition to processing traveltimes to estimate velocity, geophysicists process the amplitudes to estimate attenuation. Before the inversion is performed, the amplitudes must be adjusted to account for the source radiation pattern and the receiver radiation pattern (Bregman et al., 1989b). The inversion itself must account for the source amplitude, the receiver transfer function, and the velocity gradients (Vasco et al., 1996). Thus, the processing of amplitudes is much more complex than the processing of traveltimes, and consequently, relatively few case studies involving amplitude tomography are published. Two new techniques simplify somewhat the processing (Quan and Harris, 1997; Liu et al., 1998; Zhou and Liu, 2000).

Data interpretation

Interpretation is demonstrated with an example of field data, which is from Ellefsen et al. (1998, 2001). The field site was near Mirror Lake in central New Hampshire, and the borehole-to-borehole seismic method was one of several geophysical methods used to characterize the fractured bedrock.

At the field site, the surficial bedrock was mapped by Barton (1997) and Burton et al. (1999), and the bedrock penetrated by the wells was mapped by Johnson and Dun-

stan (1998). The bedrock consists of schist that was intruded by granite and then by pegmatite. The fracture orientation is highly variable, although there is a slight preference for strikes of 30° east and dips of 7° northwest, 50° southeast, and 82° southeast. The fracture apertures range from 0.005 to 26.6 mm; 90% of all apertures are less than 3 mm. (The smallest aperture that was measured was 0.005 mm.) The fracture trace lengths range from 1.0 to 24.6 m; 85% of the trace lengths are less than 6 m. (The smallest length that was measured was 1.0 m.) In summary, the bedrock is very heterogeneous, is cut by many small fractures, but is not cut by a large fracture zone or fault.

Borehole-to-borehole seismic data were collected and processed using the principles described in the previous subsections. A typical tomogram is shown in Figure 24. The top and the bottom edges of the tomogram are the boundaries beyond which the P-waves did not sample the bedrock enough to estimate the velocities. The left and the right edges are at the source and the receiver boreholes, respectively.

The tomographic velocities at the boreholes were compared to hydraulic conductivities, which were measured using single borehole hydraulic tests. If the velocities were high (greater than or equal to 5200 m/s), the probability was 0.05 that the rock had a high hydraulic conductivity (greater than 10^{-6} m/s). In contrast, if the velocities were low (less than 5200 m/s), the probability was 0.20 that the rock had a high hydraulic conductivity. These relations indicated that the rock rarely had a high conductivity; the reason was that the fractures themselves rarely had a high conductivity, or the fractures were rarely connected to other conductive fractures, or both. These relations also indicated that the highest probability (for a high hydraulic conductivity) occurred when the velocity was low; the reason was that the fractures lowered the velocity and tended to increase the hydraulic conductivity. (The velocity was also affected by rock type. However, the rock type between the wells was not known and consequently including it in the probabilistic relations would not have been beneficial to the interpretation of the tomograms.)

The tomogram was interpreted with these probability relations. To this end, the tomogram was divided into different regions such that, within each region, all velocities were either high or low (Figure 24b). In those regions with high velocities, the probability of high conductivity was 0.05. In those regions with low velocities, the probability of high conductivity was 0.20.

The interpreted tomogram (Figure 24b) was used to understand the results of cross-borehole hydraulic tests (Hsieh and Shapiro, 1996, 127–130). For example, one result of the tests was that a hydraulic connection existed between two intervals: 70 to 75 m depth in the source borehole and 70 to 75 m depth in the receiver borehole. These two intervals correlated with region 5 in the interpreted tomogram. Because region 5 has the higher probability (for a high hydraulic conductivity), region 5 might correspond to the hydraulic connection between the wells.

References to case histories

The borehole-to-borehole seismic method has been used for investigations related to mineral exploration, coal exploration, and assessment of mining hazards. An overview of these investigations and extensive references are given by Goulty (1993), and two field studies are summarized by Ivansson (1987). The method has been used for

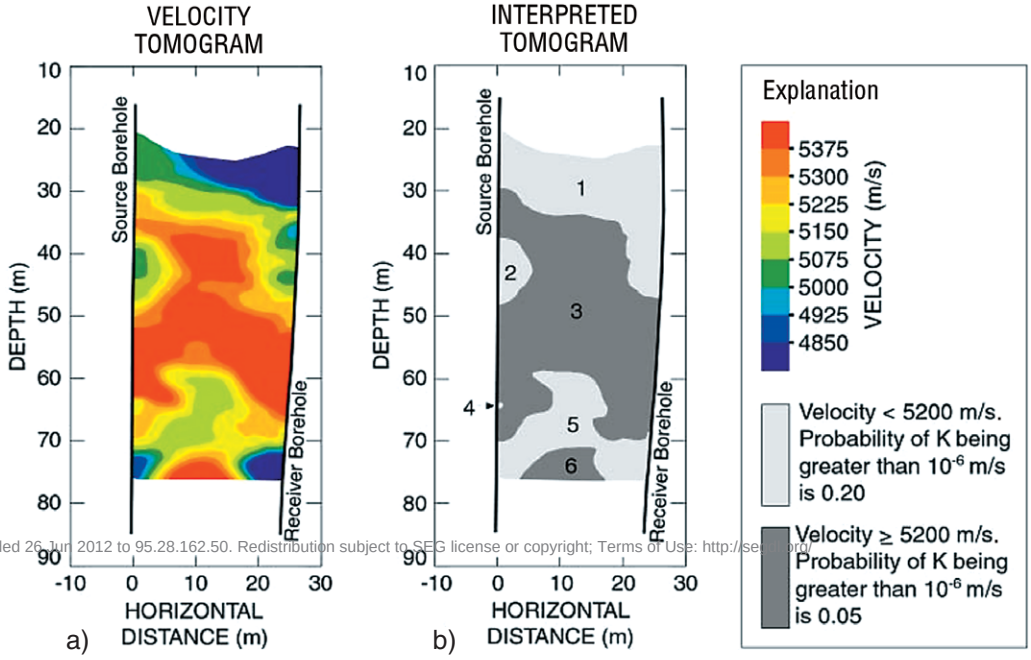

Figure 24. (a) A typical tomogram for borehole-to-borehole seismic data. (b) Interpretation of the tomogram, in terms of the likelihood of a high hydraulic conductivity (K). The numbers refer to different regions within the interpreted tomogram.

investigations related to construction of buildings, dams, nuclear repositories, and so on. An overview of these investigations and extensive references are given by Goulty (1993); a recent field study of sedimentary rocks beneath fuel storage tanks is presented by Parra et al. (1998). The method also has been used for groundwater investigations related to fractured bedrock (Bregman et al., 1989a; Majer et al., 1990, 1997; and Kaelin and Johnson, 1999) and to delineation of aquifers (Yamamoto et al., 1995; Hyndman and Harris, 1996).

The borehole-to-borehole radar method is newer than the borehole-to-borehole seismic method, and consequently, there are fewer published reports on applications of borehole-to-borehole radar. Nonetheless, this method has been used to monitor moisture in the unsaturated zone (Eppstein and Dougherty, 1998), delineate flow paths in the unsaturated zone (Hubbard et al., 1997), monitor changes in rock properties caused by underground construction (Jung and Kim, 1999), map stratigraphy in unconsolidated sediments (Wright et al., 1998), map fracture zones (Saito et al., 1988; Olsson et al., 1992; Wänstedt et al., 2000), and map fracture zones with brine tracers (Lane et al., 1998a, 1998b).

Public-domain software

Programs pick_xwell and check_picks_x are used to interactively pick and check traveltimes for borehole-to-borehole seismic and radar data (see Ellefsen (1999, 2000) for the Internet addresses). Both programs are written in the IDL programming language and execute on computers with the Unix operating system and the X-windows interface.

Before the U. S. Bureau of Mines closed, several of its geophysicists developed four computer programs to estimate velocity and attenuation for borehole-to-borehole seismic and radar data. To make these programs readily available to the public, the programs and the associated manuals are stored on a website, which is operated by the U. S. Geological Survey (see Tweeton, 2000a–2000d, for the Internet addresses). The programs execute on a personal computer; they are not maintained.

Integrating Surface and Borehole Geophysics

Surface-geophysical methods provide a useful means for the noninvasive investigation of the subsurface. Geophysical well logs are restricted to boreholes but have the advantage of providing the same geophysical measurement as the surface measurement. Thus, well logs provide a unique vehicle for relating surface measurements to the subsurface environment. In general, there are three classes of such measurements: (1) acoustic logs for comparison with seismic reflection and refraction; (2) electrical resistivity and induction logs for comparison with surface electrical soundings; and (3) density logs for comparison with gravity surveys. In addition to these direct subsurface verifications of surface interpretations, logs also provide local representations of subsurface structure that can be used in formulating the geometry (numbers of layers, dimensions of cells, etc.) of inversion models used to interpret geophysical data.

One of the most common applications of geophysical logs in the interpretation of surface-geophysical surveys is the use of an acoustic log to convert the two-way traveltime scale on a seismic section to depth (Figure 25). In some situations, this can be done qualitatively by comparing the log to the seismic section at the appropriate location. In other situations, the acoustic log may show so much detail that it may not be obvious exactly which features on the log correspond to reflectors in the seismic section. The scale mismatch is resolved in a series of steps as shown in Figure 25 (Lindseth, 1979; Stewart et al., 1982). First, the acoustic and density logs are "zoned" into sections of approximately constant value. Then, the acoustic impedance contrasts (given as a function of V_P and density in each zoned layer) are computed for each contact using the equation (White, 1983):

$$R = \frac{\rho_1 V_{P_1} - \rho_2 V_{P_2}}{\rho_1 V_{P_1} + \rho_2 V_{P_2}}, \tag{6}$$

where R is the reflection coefficient, and ρ_1 and ρ_2 and V_{P1} and V_{P2} are the density and P-wave velocity above and below the contact. The impedance contrasts are concentrated at precise depth points. Each of these values is then convolved with a wavelet representative of the source used in the seismic survey, resulting in a *synthetic seismogram* for the borehole location. This synthetic trace can be inserted into the seismic section, the scales adjusted until a match is made, and the relation between two-way traveltime and depth identified.

In many studies, the surface measurements can effectively define the distribution of subsurface properties such as electrical conductivity or density, but the relation between those quantities and the physical property of interest may be uncertain. In an example from an alluvial aquifer in Montana, surface electrical induction soundings indicated anomalously high electrical conductivity in the subsurface. Geophysical logs were used to calibrate (Figure 26) these measurements in units of direct interest (specific electrical conductance of water samples), because boreholes allow direct regression between water-sample conductance and the conductance of the aquifer from which they are derived (Kwader, 1985; Paillet et al., 1999a). In Figure 26, the induction log samples the conductivity of small volumes derived directly from the aquifer. The induction conductivity can be averaged over the screened interval in the sampling well to gen-

erate a regression between formation conductivity and water-sample conductance. This regression can be used to calibrate the surface electrical soundings in units of pore water electrical conductance. Note that this regression applies only to the aquifer zones. The log data also provide an interpretation model indicating the depth interval over which calibration applies. The effect of overlying sand and clay and underlying shale on bulk electrical conductivity soundings must also be included in the interpretation model. This is yet another example of the way in which having more than one physically independent borehole measurement (in this case, gamma and induction) can be used to resolve the dependence of one geophysical measurement on more than one physical property of the subsurface.

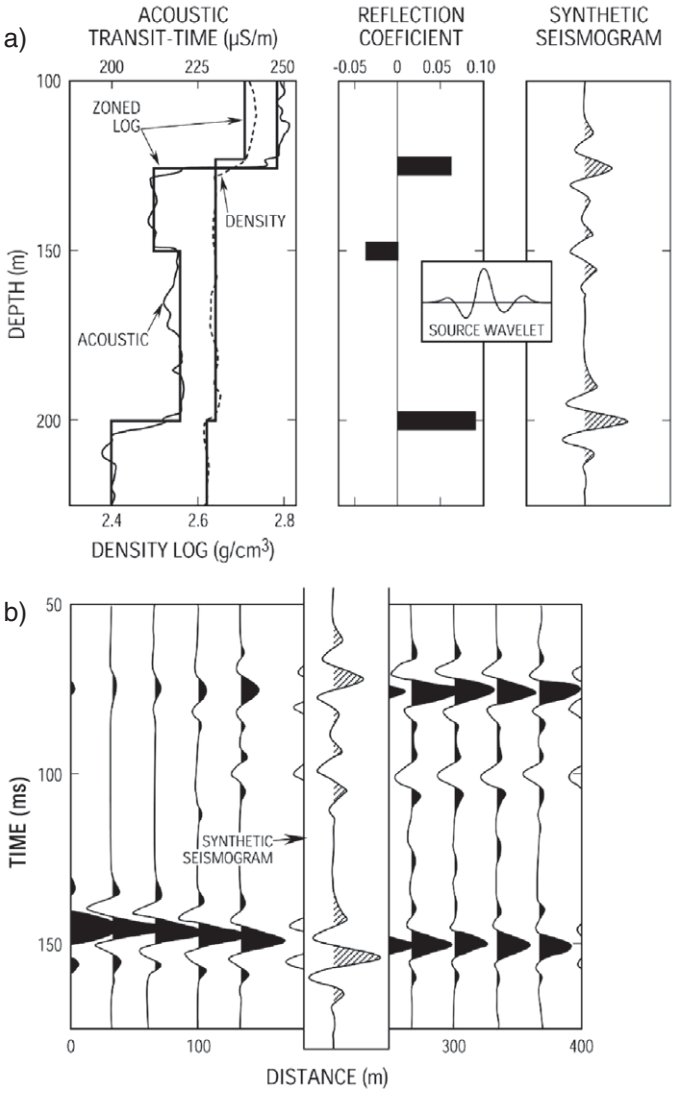

Figure 25. Schematic illustration of steps in the integration of surface and borehole seismic data: (a) Generation of a synthetic seismogram from zoned acoustic and density log data; and (b) insertion of a synthetic seismic trace with its depth scale onto the seismic section plotted in units of two-way traveltime (adapted from Hearst et al., 2000).

Summary

Geophysical measurements in boreholes have the advantage of providing detailed profiles of subsurface properties and the disadvantage of being restricted to locations where boreholes are available. Although geophysical well logs, in theory, measure the properties of the geological formation in situ, logs have to be corrected for the

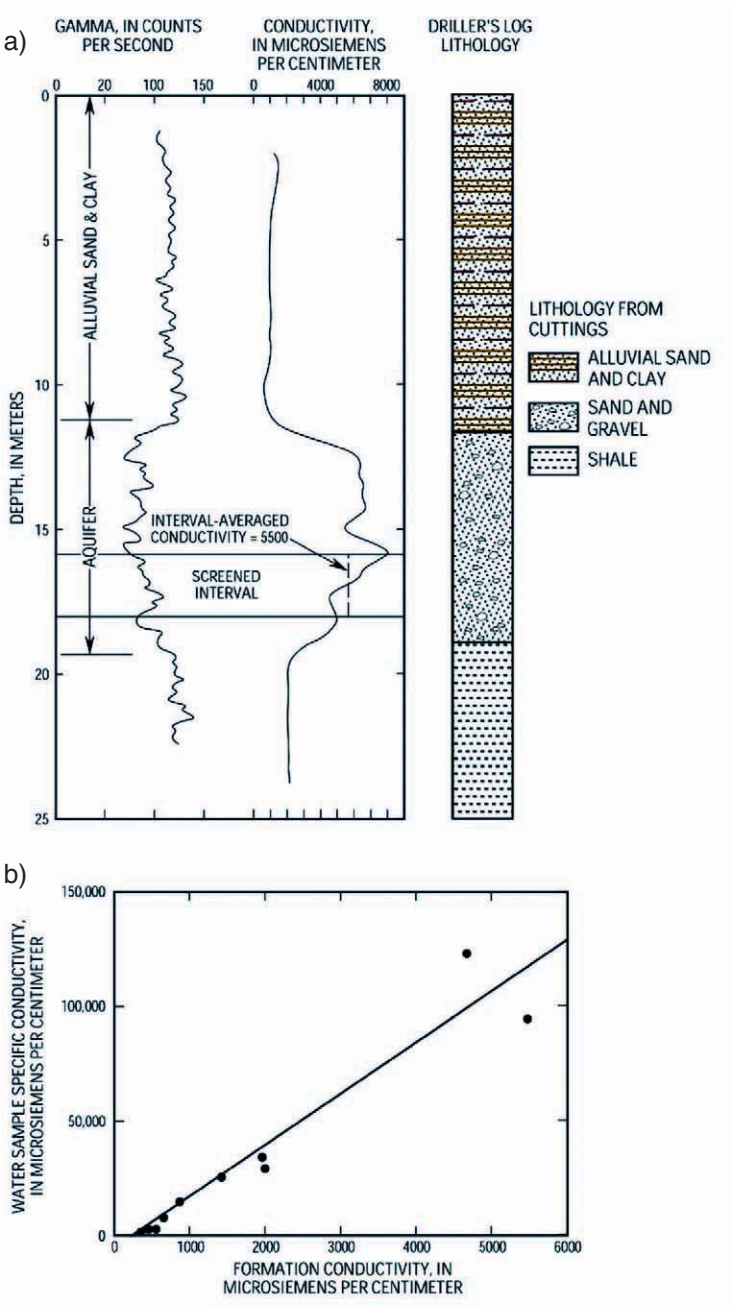

Figure 26. (a) Gamma and induction logs show the location of the aquifer and indicate the average formation conductivity of the screened interval in a water-sampling well; and (b) interval-averaged formation induction regressed against the specific electrical conductivity of the sampled water (Paillet, 1995).

effects of the borehole, casing and annulus (if present), and drilling damage or invasion. Selection of geophysical well logging equipment suitable for a specific borehole environment is important, ranging from miniature direct-push probes inserted into the soil to large-diameter probes suitable for use in water-supply production wells. Conventional well logs are used most effectively when they are combined with other information such as drillers' logs, core descriptions, and water sample data. The tremendous mismatch between the scales of investigation of surface geophysical measurements and borehole logs provides a unique way to investigate the effect of scale on the physical properties of the subsurface. The latest borehole geophysical technology also provides ways to address intermediate scales by controlling the depth of investigation of a geophysical logging probe (i.e., electrode spacing in normal resistivity), and through cross-borehole methods and borehole directional radar logging.

Appendix A
Overdetermined Inversion for Porosity Using Nuclear Logs

Calibrated neutron-porosity and gamma-gamma density logs are given in Figure A-1 for the sandstone and shale sequence of Figure E-1. The neutron log is calibrated directly in porosity units. The density log is converted to porosity units by assuming the density of fresh water filling pore spaces and the density of quartz for the sandstone matrix. As in previous interpretations involving multiple lithologies, no single log can be used to give an effective interpretation of porosity. The effects of lithology (sandstone versus shale) is incorporated by assuming a noneffective neutron porosity for the shale (which must be subtracted from the log measurement to give "true" porosity) and by recognizing that the grain density of shale is different from the gain density of quartz. These two parameters are treated as *calibration constants* in the geophysical inversion but are actually unknown. The analysis treats the neutron and density log interpretations as the inversion of two equations (neutron and density data) for a single unknown (porosity). This is a typical over-determined inversion, where the residual is the root mean square (rms) sum of the difference between the two porosity interpretations at each depth point on the logs in Figure A-1. Minimization of the residual summed over the entire depth interval results in the plots shown in the figure, where the noneffective porosity of the shale is 20%, and the grain density of the shale mineral is 2.50 g/cm^3. The one place where the two logs significantly disagree (319–322 m interval) corresponds to a small limestone bed where the assumption of the inversion scheme (sandstone and shale lithology) does not apply.

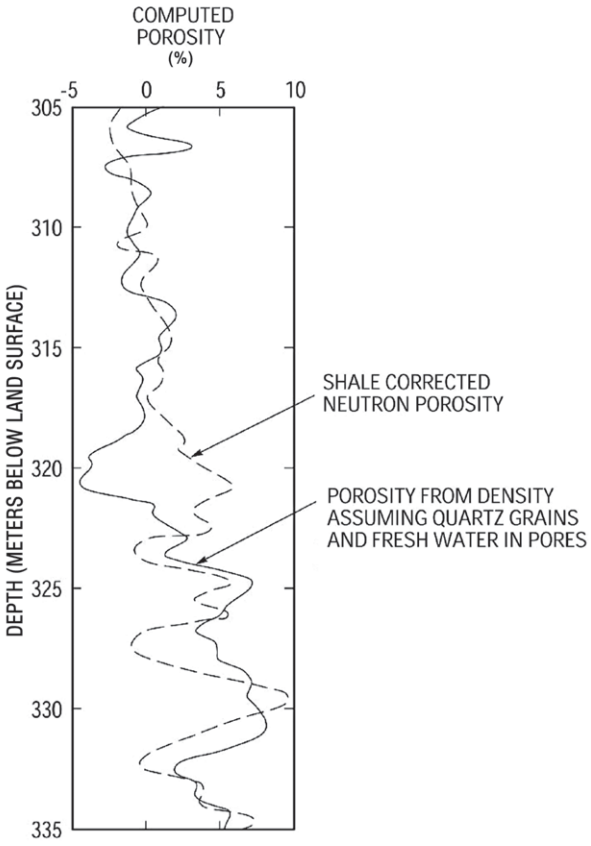

Figure A-1. Calibrated neutron porosity and gamma density logs, where the gamma density has been converted to porosity using estimated density for quartz sand and indurated shale; this is the same sand and shale sequence illustrated in Figure E-1 (Paillet and Crowder, 1996).

Appendix B
Gamma Log Used to Identify Aquifers for Monitoring

Figure B-1 shows the gamma log from an auger-drilled borehole in glacial sediments. The log indicates gamma activity that can be tied to the physical description of sediments given by the driller. The drilling report contains an accurate description of the sediments but does not provide very accurate depths for contacts. In contrast, the log gives accurate depths but only indicates gamma activity. The figure shows the expected relation between gamma activity and clay fraction because the gamma high at about 24 m in depth corresponds to a lake-bed clay. However, the gamma high at about 8 m in depth corresponds to an unweathered granite cobble in till and not clay. This is a clear demonstration of the fact that all sediment properties cannot be represented along a single scale of gamma activity. Thus, this single log indicates both the advantages and disadvan-

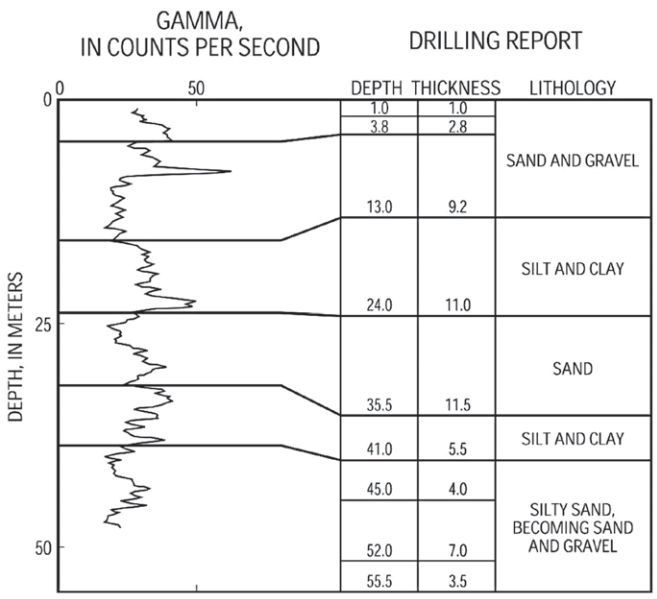

Figure B-1. Gamma log in glacial sediments correlated with a detailed description of sediments encountered during drilling.

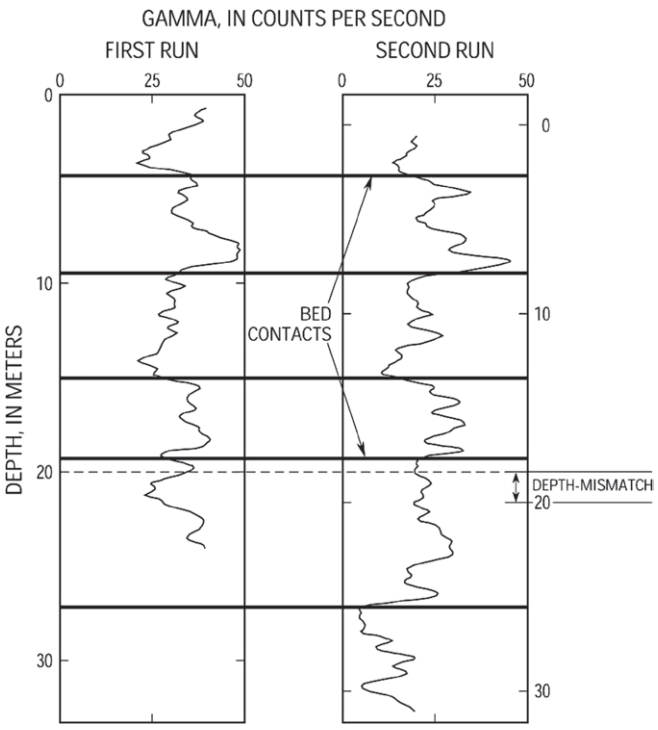

Figure C-1. Repeated gamma logs obtained in alluvial sediments illustrating depth correlation of logs and repeatability of logs influenced by nuclear statistical characteristics.

tages of using geophysical logs to identify aquifers. Best results are obtained when both geological descriptions and geophysical logs are used.

Appendix C
Repeat Gamma Logs Used as a Quality Control

Figure C-1 shows a typical example of a repeated log section used to ensure quality control in a gamma log interpretation. This example shows that beds are repeated, while there are some variations in detail in the logs that can be attributed to nuclear statistical noise. The two logs also show a depth error (depth mismatch). Which log has the proper depth scale? Such errors usually occur because the logging cable has lost tension during lowering of the probe. This causes the cable to move without recording a depth change in the log record. In this example, the gamma probe was caught on a "ledge" at the top of the well screen during the initial run, but tension was maintained so that the log obtained during the return of the probe to the surface had an accurate depth scale. This was verified because the depth indicator showed zero when the probe returned to the reference point. Less care was taken on the second run when the probe caught momentarily at the top of the screen, and cable tension was lost for a short time. When the log was repeated on a second run, the probe descended into the screen, but a depth error was incurred. As a result, the probe was actually slightly deeper than the depth registered by the logging equipment when a log was recorded while bringing the probe up on the second run. Therefore, the log on the right has been adjusted (moved downward) to account for such a depth error (the log should read deeper than indicated on the depth scale).

The depth error in Figure C-1 points out two important logging practices. First, logs are almost always obtained while pulling the probe upwards. The upward logging procedure insures that there is uniform tension on the cable and uniform motion of the probe. Second, it is also important to verify that the probe returns to the nominal depth reference point at the end of the logging run. Verification that the depth at the end of logging agrees with the reference depth defined at the start of logging is a critical quality control step usually included with a repeated log section as part of a standard logging service contract (Bateman, 1985; Theys, 1994). Such a check on the zero reference for the example in Figure C-1 verified that a depth error had been incurred during the second gamma log run.

Appendix D
Using Geophysical Logs to Estimate the Quality of Groundwater In Situ

One of the most important applications of well logs is the use of log data to infer the properties of groundwater in situ, as distinguished from the properties of water filling a

borehole at a given depth (Figure D-1) (Kwader, 1985). In this example, a municipal water well produced brackish water when pumped, but water sampled from the well with the pump removed was fresh. The supply well was completed with steel casing down to 200 m, with an open hole enlarged by explosives below that point. A suite of logs from this well show unambiguously that the well was filled with fresh water, but the formation surrounding the well was saturated with brackish water below a depth of about 400 m. Local variations in formation resistivity are clearly related to shale fraction as indicated by the gamma log. However, the long-normal resistivity (162.6 cm measurement electrode spacing) log shows a baseline shift to significantly lower resistivity below about 400 m. The short-normal (40.6 cm measurement electrode spacing) log does not show this change very well because the borehole diameter is greater than the electrode spacing on the short-normal sonde. The presence of fresh water throughout the borehole is attributed to flow along the well bore, with flow entering above 300 m and exiting below 425 m. Although flow measurements could not be made in this well, the stepped nature of the fluid column temperature and resistivity logs strongly suggest that such flow existed at the time of logging. The fluid electrical conductivity log was used to estimate the specific conductance of water inflowing from the upper part of the aquifer (350 µS/cm). This value was then combined with the long-normal resistivity log data to estimate a formation factor of about 40. This formation factor estimate was used to give an estimate of groundwater specific conductance for the lower part of the aquifer of about 2800 µS/cm, corresponding to about 1900 mg/l total dissolved solids. Note that in carrying out these calculations, formation resistivity is not simply read from the logs. The long-normal data were first corrected to account for the effects of the borehole fluid using departure curves, and then adjusted to correspond with values at a standard temperature of 25°C.

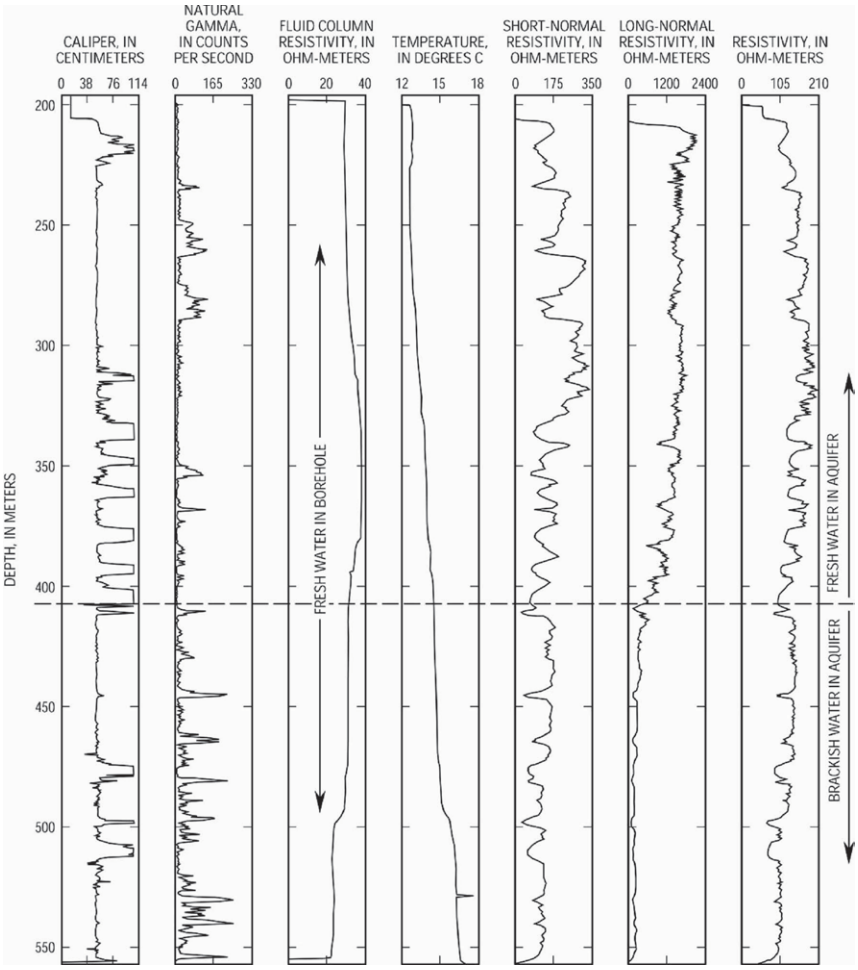

Figure D-1. Geophysical logs from a water supply well in Wisconsin indicate that the well itself is filled with fresh water, but the formation below about 400 m in depth is saturated with brackish water that enters the well during pumping.

Appendix E
Acoustic Porosity Log Application

A typical acoustic velocity log (sometimes denoted as the *sonic* log) is compared to other logs for a sandstone and shale aquifer sequence in Figure E-1. Acoustic logs are often plotted with transit time increasing towards the left, so that acoustic velocity increases to the right. The transit-time scale is used because acoustic logs are interpreted in porosity units on the basis of the Wyllie transit-time equation (Wyllie et al., 1958):

$$DT = (1-\Phi)\,DT_R + \Phi DT_W,$$

where DT is the measured P-wave transit time, Φ is porosity, and DT_R and DT_w are the transit times of the rock matrix and pore water. In practice, the main difficulty in using this expression is that DT_R varies with depth of burial (confining pressure) for one lithology and also varies with lithology. In Figure E-1, the lithology is an upward-fining sandstone and shale unit. Clean sandstone corresponds to the gamma lows near the bottom of the section, and core porosity values are available for these sandstone sections. The acoustic log calibration shows the porous sandstone sections correspond to the lowest nominal porosities in the

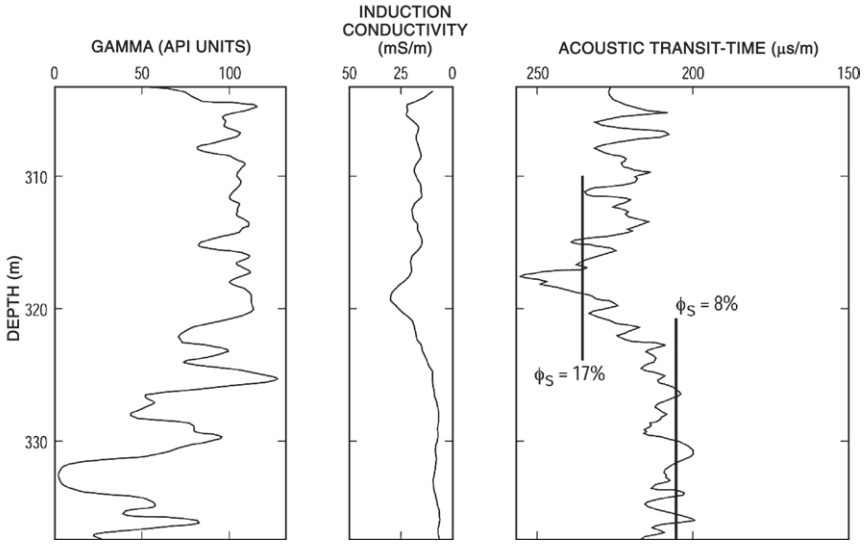

Figure E-1. Acoustic log for a sandstone and shale formation compared to gamma and induction logs, where ϕ denotes the sandstone porosity interpreted from the Wyllie transit-time equation under the standard assumptions of quartz mineral grains and fresh water saturating all pore spaces.

interval if the DT_R is taken as 170 μs/m typical of quartz. The acoustic-log porosity of the upper section appears higher only because the calculation assumes a constant DT_R, whereas the rock fabric varies from sandstone to mostly shale. This is another affirmation of the fact that several different well logs need to be combined to provide an effective interpretation of formation properties. Once nonaquifer shale units are removed from the intervals of interest using the other log data, comparison with core data confirms that the aquifer section has effective porosity values ranging from 5 to 12%, and averaging about 8%.

References

Aki, K., and P. G. Richards, 1980, Quantitative seismology, Theory and methods, Vols. 1 and 2: W. H. Freeman and Co.

ASTM, 1995, Standard guide for planning and conducting borehole geophysical logging: American Society for Testing and Materials, D 5753.

Barton, C. C., 1997, Bedrock geologic map of Hubbard Brook Experimental Forest and maps of fractures and geology in roadcuts along Interstate 93, Grafton County, New Hampshire: U. S. Geological Survey Miscellaneous Investigations Series Map I-2562, 2 sheets, scale 1–12000.

Bateman, R. M., 1985, Cased-hole log analysis and reservoir performance monitoring: International Human Resources Development Corp.

Beydoun, W. B., C. H. Cheng, and M. N. Toksöz, 1985, Detection of open fractures with vertical seismic profiling: Journal of Geophysical Research, **90**, 4557–4566.

Biella, G., A. Lozeij, and I. Tabacco, 1983, Experimental study of some hydrogeological properties of unconsolidated porous media: Ground Water, **21**, 741.

Born, M., and E. Wolf, 1989, Principles of optics—Electromagnetic theory of propagation, interference and diffraction of light: Pergamon Press, Inc.

Bradley, J. A., and D. L. Wright, 1987, Microprocessor-based data-acquisition system for a borehole radar: IEEE Trans. Geoscience Remote Sensing, **GE-25**, 441–447.

Bregman, N. D., R. C. Bailey, and C. H. Chapman, 1989a, Crosshole seismic tomography: Geophysics, **54**, 200–215.

Bregman, N. D., C. H. Chapman, and R. C. Bailey, 1989b, Travel time and amplitude analysis in seismic tomography: Journal of Geophysical Research, **94**, 7577–7587.

Brock, J., 1986, Applied open-hole log analysis: Gulf Publishing Co.

Burton, W. C., T. R. Armstrong, and G. J. Walsh, 1999, Bedrock geologic framework of the Mirror Lake Research Site, New Hampshire, *in* D. W. Morganwalp, and H. T. Buxton, eds., U. S. Geological Survey Toxic Substances Hydrology Program—Proceedings of the technical meeting: U. S. Geological Survey Water-Resources Investigations Report 99-4018C, 705–713.

Chapman, C. H., and R. G. Pratt, 1992, Traveltime tomography in anisotropic media—I. Theory: Geophysics Journal International, 109, 1–19.

Chen, S. T., 1989, Shear-wave logging with multipole sources: Geophysics, **54**, 590–597.

Cicerone, R. D., 1991, Detection and characterization of in-situ fractures in the earth from vertical seismic profiling data: Ph.D. dissertation, Massachusetts Institute of Technology.

Crampin, S., 1987, Geological and industrial implications of extensive-dilatancy anisotropy: Nature, **328**, 491–496.

Crampin, S., E. M. Chesnokov, and R. G. Hipkin, 1984,

Seismic anisotropy—The state of the art—II: Geophysics Journal of the Royal Astronomical Society, **76**, 1–16.

Daily, W., A. Ramirez, D. LaBrecque, and W. Barber, 1995, Electrical resistance tomography experiments at the Oregon Graduate Institute: Applied Geophysics, **33**, 227–237.

Doveton, J. H., 1986, Log analysis of subsurface geology: John Wiley & Sons, Inc.

Dubois, J. C., 1995, Borehole radar experiment in limestone—Analysis and data processing: First Break, **13**, 57–67.

Ebihara, S., M. Sato, and H. Niitsuma, 1998, Analysis of a guided wave along a conducting structure in a borehole: Geophysical Prospecting, **46**, 489–505.

Ekstrom, M. P., et al., 1987, Formation imaging with microelectrical scanning arrays: Log Analyst, **28**, 294–306.

Ellefsen, K. J., 1999, pick_xwell: A program for interactive picking of crosswell seismic and radar data: U. S. Geological Survey Open-File Report 99–534, available at http://greenwood.cr.usgs.gov/pub/open-file-reports/ofr-99-0534/.

Ellefsen, K. J., 2000, check_picks_x: A program for checking the travel time picks of crosswell seismic and radar data: U. S. Geological Survey Open-File Report 00-109, available at http://greenwood.cr.usgs.gov/pub/open-file-reports/ofr-00-109/.

Ellefsen, K. J., P. A. Hsieh, and A. M. Shapiro, 2002, Crosswell seismic investigation of hydraulically conductive, fractured bedrock near Mirror Lake, New Hampshire: Journal of Applied Geophysics, **50**, 299–317.

Ellefsen, K. J., J. E. Kibler, P. A. Hsieh, and A. M. Shapiro, 1998, Crosswell seismic tomography at the USGS Fractured Rock Research site: Data collection, data processing and tomograms: U. S. Geological Survey Open-File Report 98–510.

Ellis, D. V., 1987, Well logging for earth scientists: Elsevier Science Publishing Co., Inc.

Endres, A. L., and W. P. Clement, 1998, Relating cone penetrometer test information to geophysical data—A case study, *in* R. S. Bell, M. H. Powers, and T. Larson, eds., Proceedings of the Symposium on the Application of Geophysics to Engineering and Environmental Problems: Environmental and Engineering Geophysics Society, 295–303.

Eppstein, M. J., and D. E. Dougherty, 1998, Efficient three-dimensional data inversion: Soil characterization and moisture monitoring from cross-well ground penetrating radar at a Vermont test site: Water Resources Research, **34**, 1889–1900.

Gibson, R. L. Jr., 1994, Radiation from seismic sources in cased and cemented boreholes: Geophysics, **59**, 518–533.

Gilmore, R. J., B. Cark, and D. Best, 1987, Enhanced saturation determination using the EPT-G endfire antenna array: Transactions of the 28th Annual Logging Symposium, Society of Professional Well Log Analysts, paper K.

Goulty, N. R., 1993, Controlled-source tomography for mining and engineering applications, *in* H. M. Iyer, and K. Hirahara, eds., Seismic tomography—Theory and practice: Chapman and Hall.

Hardin, E. L., Cheng, C. H., Paillet, F. L., and Mendelson, J. D., 1987, Fracture characterization by means of attenuation and generation of tube waves in fractured crystalline rock at Mirror Lake, New Hampshire: Journal of Geophysics Research, **92**, 7989–8006.

Hearst, J. R., P. H. Nelson, and F. L. Paillet, 2000, Well logging for physical properties, 2nd ed.: John Wiley and Sons, Inc.

Hess, A. E., 1986, Identifying hydraulically conductive fractures with a slow-velocity borehole flowmeter: Canadian Geotechnical Journal, **23**, 69–78.

Hodges, R. E., 1988, Calibration and standardization of geophysical well-logging equipment for hydrologic applications: U. S. Geological Survey Water-Resources Investigations Report 92-4090.

Holliger, K., and T. Bergmann, 2000, Finite difference modeling of borehole georadar data, *in* D. Noon, G. Stickley, and D. Longstaff, eds., Proceedings of the 8th International Conference on Ground Penetrating Radar.

Hsieh, P. A., and A. M. Shapiro, 1996, Hydraulic characteristics of fractured bedrock underlying the FSE well field at the Mirror Lake site, Grafton County, New Hampshire, *in* D. W. Morganwalp, and D. A. Aronson, eds., U.S. Geological Survey Toxic Substances Hydrology Program—Proceedings of the technical meeting: U. S. Geological Survey Water-Resources Investigations Report 94-4015, 127–130.

Hubbard, S. S., et al., 1997, Estimation of permeable pathways and water content using tomographic radar data: The Leading Edge, **16**, 1623–1628.

Hubbard, S. S., Y. Rubin, and E. Majer, 1999, Spatial correlation structure estimation using geophysical and hydrogeological data: Water Resources Research, **35**, 1809–1825.

Hurst, A., M. A. Lovell, and A. C. Morton, 1990, Geological applications of wireline logs: Geological Society.

Hyndman, D. W., and J. M. Harris, 1996, Traveltime inversion for the geometry of aquifer lithologies: Geophysics, **61**, 1728–1737.

Ivansson, S., 1987, Crosshole transmission tomography, *in* G. Nolet, ed., Seismic tomography with applications in global seismology and exploration geophysics: D. Reidel Publishing Co., 159–188.

Jacobsen, L., R. Beals, D. F. Wyatt Jr., and A. Hrametz, 1993, Response characterization of an induced gamma spectrometer tool using a bismuth germanate scintillator: Log Analyst, **34**, 14–22.

Johnson, C. D., and A. H. Dunstan, 1998, Lithology and fracture characterization from drilling investigations in the Mirror Lake area, Grafton County, New Hampshire: U. S. Geological Survey Water-Resources Investigations Report 98-4183.

Jorgensen, D. G., 1991, Estimating geohydrologic properties from corehole geophysical logs: Ground Water Monitoring and Remediation **10**, 69–78.

Jung, Y., and J. Kim, 1999, Application of anisotropic georadar tomography to monitor rock physical property changes: Journal of Environmental and Engineering Geophysics, **4**, 87–92.

Kaelin, B., and L. R. Johnson, 1999, Using seismic crosswell surveys to determine the aperture of partially water-saturated fractures: Geophysics, **64**, 13–23.

Kearal, P. M., 1997, Observations of particle movement in a monitoring well using the colloidal boroscope: Journal of Hydrology, **200**, 323–344.

Kenyon, W. E., 1997, Petrophysical applications of NMR logging: Log Analyst, **38**, 21–29.

Keys, W. S., 1986, Analysis of geophysical logs of water wells with a microcomputer: Ground Water, **24**, 750–760.

Keys, W. S., 1990, Borehole geophysics applied to groundwater investigations: U. S. Geological Survey Techniques of Water-Resources Investigations, Book 2, Chap. E2.

King, R. W. P., G. S. Smith, M. Owens, and T. T. Wu, 1981, Antennas in matter—Fundamentals, theory, and applications: Massachusetts Institute of Technology Press.

Kitsunezaki, C., 1980, A new method for shear wave logging: Geophysics, **45**, 1489–1506.

Kwader, T., 1985, Estimating aquifer permeability from formation resistivity factor: Ground Water, **23**, 762–766.

LaBrecque, D. J., G. Morelli, and P. Lundegard, 1996, Monitoring air sparging in complex aquifers, *in* Proceedings of the Symposium on the Application of Geophysics to Engineering and Environmental Problems: Environmental and Engineering Geophysics Society, 733–742.

Lane, J. W., F. P. Haeni, F. D. Day-Lewis, 1998a, Use of time-lapse attenuation-difference radar tomography methods to monitor saline trace transport in fractured crystalline bedrock: Proceedings of the Seventh International Conference on Ground-Penetrating Radar, 27-30 May 1998, Lawrence, Kansas, 533–538.

Lane, J. W., P. K. Joesten, F. P. Haeni, M. Vendl, and D. Yeskis, 1998b, Use of borehole-radar methods to monitor the movement of a saline tracer in carbonate rock at Belvidere, Illinois: Proceedings of the Symposium on the Application of Geophysics to Engineering and Environmental Problems, 323–332.

Lee, M. W., and A. H. Balch, 1982, Theoretical seismic wave radiation from a fluid-filled borehole: Geophysics, **47**, 1308–1314.

Lindseth, R. O., 1979, Synthetic sonic logs—A process for stratigraphic interpretation (reflection coefficient): Geophysics, **44**, 3.

Liu, L., J. W. Lane, and Y. Quan, 1998, Radar attenuation tomography using the centroid frequency downshift method: Journal of Applied Geophysics, **40**, 105–116.

Lo, T., and P. L. Inderwiesen, 1994, Fundamentals of seismic tomography: Society of Exploration Geophysicists.

Lofts, J. P., P. K. Harvey, and M. A. Lovell, 1993, The characterization of reservoir rocks using nuclear logging tools: Evaluation of mineral transform techniques in the laboratory and log environments: Log Analyst, **36**, 16–24.

Long, J. C. S., et al., 1996, Rock fractures and fluid flow—Contemporary understanding and applications: National Academy Press.

Lynch, E. J., 1962, Formation evaluation: Harper and Row.

Lytle, R. J., and K. A. Dines, 1980, Iterative ray tracing between boreholes for underground image reconstruction: IEEE Transactions on Geoscience and Remote Sensing, **GE-18**, 234–239.

Majer, E. L., et al., 1990, Joint seismic, hydrogeological, and geomechanical investigations of a fracture zone in the Grimsel Rock Laboratory, Switzerland: NAGRA TR 90-49, Swiss National Cooperative for Radioactive Waste Disposal (NAGRA).

Majer, E. L., et al., 1997, Fracture detection using crosswell and single well surveys: Geophysics: **62**, 495–504.

Maurer, H. R., 1996, Systematic errors in seismic crosshole data—Application of the coupled inverse technique: Geophysical Research Letters, **23**, 2681–2684.

McCall, W., and P. Zimmerman, 2000, Direct push electrical and CPT logging—An introduction: Proceedings of the 7th International Symposium on Borehole Geophysics for Minerals, Geotechnical, and Groundwater Applications, 103–114.

Meredith, J. A., 1990, Numerical and analytical modeling of downhole seismic sources—The near and far field: Ph.D. dissertation, Massachusetts Institute of Technology.

Meredith, J. A., M. N. Toksöz, and C. H. Cheng, 1993, Secondary shear waves from source boreholes: Geophysical Prospecting, **41**, 287–312.

Milsom, J., 1989, Field Geophysics: Halsted Press: John Wiley and Sons, Inc.

Mitchell, J. K., and T. L. Brandon, 1998, Analysis and use of CPT in earthquake environmental engineering: Proceedings of the First International Conference On Site Characterization—ISC '98, 1, 69–97.

Molz, F. J., G. K. Bowman, S. C. Young, and W. R. Waldrop, 1994, Borehole flowmeters—Field application

and data analysis: Journal of Hydrology, **163**, 347–371.

Newhouse, M. W., and R. T. Hansen, 2000, Application of three-dimensional borehole flow measurements to the analysis of seawater intrusion and barrier injection systems: Proceedings of the 7th International Symposium on Borehole Geophysics for Minerals, Geotechnical, and Groundwater Applications, 281–292.

Nolet, G., 1985, Solving or resolving inadequate and noisy tomographic systems: J. Comput. Phys., **61**, 463–482.

Oden, C. P., J. R. Stowell, and J. J. LoCoco, 2000, Variable frequency monopole-dipole sonic logging for shear velocity—Applications and test results: Proceedings of the 7th International Symposium on Borehole Geophysics for Minerals, Geotechnical, and Groundwater Applications, 71–76.

Olsson, O., L. Falk, O. Forslund, L. Lundmark, and E. Sandberg, E., 1992, Borehole radar applied to the characterization of hydraulically conductive fracture zones in crystalline rock: Geophysical Prospecting, **40**, 109–142.

Paige, C. C., and M. A. Saunders, 1982, LSQR—An algorithm for sparse linear equations and sparse least squares: ACM Transactions on Mathematical Software, **8**, 43–71.

Paillet, F. L., 1995, Integrating surface geophysics, well logs, and hydraulic test data in the characterization of heterogeneous aquifers: Journal of Environmental and Engineering Geophysics, **0**, 1–13.

———2000, A field technique for estimating aquifer parameters using flow log data: Ground Water, **38**, 510–521.

Paillet F. L., and D. Boyce, 1996, Analysis of well logs for borehole ANL-OBS-A-001 at the Idaho National Engineering Laboratory, Idaho: U. S. Geological Survey Open-File Report 96-213.

Paillet, F. L., and C. H. Cheng, 1986, A numerical investigation of head waves and leaky modes in fluid-filled boreholes: Geophysics, **51**, 1438–1449.

———1991, Acoustic waves in boreholes—The theory and application of acoustic full-waveform logs: CRC Press.

Paillet, F. L., C. H. Cheng, and W. D. Pennington, 1992, Acoustic waveform logging—advances in theory and application: Log Analyst, **33**, 239–258.

Paillet, F. L., and R. E. Crowder, 1996, A generalized approach for the interpretation of geophysical well logs in ground water studies—Theory and application: Ground Water, **34**, 883–898.

Paillet, F. L., L. Hite, and M. Carlson, 1999a, Integrating surface and borehole geophysics in ground water studies—An example using electromagnetic soundings in south Florida: Journal of Environmental and Engineering Geophysics, **4**, 45–55.

Paillet, F. L., R. T. Kay, D. Yeskis, and W. Pedler, 1993, Integrating well logs into a multiple-scale investigation of a fractured sedimentary aquifer: Log Analyst, **34**, 13–23.

Paillet, F. L., and W. H. Pedler, 1996, Integrated borehole logging methods for wellhead protection applications: Eng. Geol., **42**, 155–165.

Paillet, F. L., and R. S. Reese, 2000, Integrating borehole logs and aquifer tests in aquifer characterization: Ground Water, **38**, 713–725.

Paillet, F. L., and J. E. White, 1982, Acoustic modes of propagation in the borehole and their relationship to rock properties: Geophysics, **47**, 1215–1228.

Paillet, F. L., J. H. Williams, and A. E. Hess, 1999b, A wireline-operated downhole packer for hydraulic measurements in boreholes: Proceedings of the Symposium on the Application of Geophysics to Engineering and Environmental Problems, 841–850.

Parker, R. L., 1994, Geophysical inverse theory: Princeton University Press.

Parra, J. O., V. Price, C. Addington, B. J. Zook, and R. J. Cumbest, 1998, Interwell seismic imaging at the Savannah River Site, South Carolina: Geophysics, **63**, 1858–1865.

Peng, C., C. H. Cheng, and M. N. Toksöz, 1993, Borehole effects on downhole seismic measurements: Geophysical Prospecting, **41**, 883–912.

———1994, Cased borehole effects on downhole seismic measurements: Geophysical Prospecting, **42**, 777–811.

Peterson, J. E., B. N. P. Paulson, and T. V. McEvilly, 1985, Applications of algebraic reconstruction techniques to crosshole seismic data: Geophysics, **50**, 1566–1580.

Pirson, S. J., 1963, Handbook of well log analysis: Prentice-Hall, Inc.

Pratt, R. G., and C. H. Chapman, 1992, Traveltime tomography in anisotropic media—II. Application: Geophysics Journal International, **109**, 20–37.

Pratt, R. G., W. J. McGaughey, and C. H. Chapman, 1993, Anisotropic velocity tomography: A case study in a near-surface rock mass: Geophysics, **58**, 1748–1763.

Quan, Y., and J. M. Harris, 1997, Seismic attenuation tomography using the frequency shift method: Geophysics, **62**, 895–905.

Ramirez, A., W. Daily, A. Binley, and D. LaBrecque, 1996, Tank leak detection using electrical resistance methods, *in* Proceedings of the Symposium on the Application of Geophysics to Engineering and Environmental Problems: Environmental and Engineering Geophysics Society, 763–772.

Reiter, D. T., and W. Rodi, 1996, Nonlinear waveform tomography applied to crosshole seismic data: Geophysics, **61**, 902–913.

Robertson, P. K., and R. G. Campanella, 1983, Interpreta-

tion of cone penetration tests—Part I (Sand) and Part II (Clay): Canadian Geotechnical Journal, 20.

Rossi, G., and C. Peroni, 1989, Apparatus for the in-situ determination of physical-chemical parameters across the sediment-water interface: Environmental Technology Letters, **10**, 511–520.

Saito, H., 1991, Anisotropic traveltime tomography at the Buckhorn test facility in Illinois: 60th Annual International Meeting, Society of Exploration Geophysicists, Expanded Abstracts, 123–126.

Saito, H., H. Shima, T. Toshioka, and H. Ohtomo, 1988, Application of geotomography techniques to site investigations for civil engineering purposes: 58th Annual International Meeting, Society of Exploration Geophysicists, Expanded Abstracts, 324–327.

Sato, M., and R. Thierbach, 1991, Analysis of a borehole radar in cross-hole mode: IEEE Transacting Geoscience and Remote Sensing, **29**, 899–904.

Scales, J. A., 1987, Tomographic inversion via the conjugate gradient method: Geophysics, **52**, 179–185.

Sirles, P. C., and A. Viksne, 1990, Site-specific shear wave velocity determinations for geotechnical engineering applications, *in* S. H. Ward, ed., Geotechnical and Environmental Geophysics, Vol. III, Geotechnical: Society of Exploration Geophysicists.

SPWLA, 1975, Glossary of terms and expressions used in well logging: Society of Professional Well Log Analysts.

Stewart, M. T., T. Lizanec, and M. Layton, 1982, Application of DC resistivity surveys to regional hydrogeologic investigations, Collier County, Florida: South Florida Water Management District.

Stumm, F., F. Paillet, J. H. Williams, and J. W. Lane, 2000, Geohydrologic assessment of crystalline bedrock for the New York City Water-Tunnel Project by use of advanced borehole-geophysical methods: Proceedings of the 7th International Symposium on Borehole Geophysics for Minerals, Geotechnical, and Groundwater Applications, 19–27.

Summers, G. C., and R. A. Broding, 1952, Continuous velocity logging: Geophysics, **27**, 598–614.

Theys, P. P., 1994, A serious look at repeat sections, *in* Transactions of the Society of Professional Well Log Analysts 16th Logging Symposium, paper GG.

Tillard, S., 1994, Radar experiments in isotropic and anisotropic geological formations (granite and schist), Geophysical Prospecting, **42**, 615–636.

Tsang, C. F., P. Hufschmied, and F. V. Hale, 1990, Determination of fracture inflow parameters with a borehole fluid conductivity method: Water Resources Research, **26**, 561–578.

Tura, M. A. C., L. R. Johnson, E. L. Majer, and J. E. Peterson, 1992, Application of diffraction tomography to fracture detection: Geophysics, **57**, 245–257.

Tweeton, D. R., 2000a, Program BOMTOM for crosswell radar and seismic tomography: U. S. Geological Survey Open-File Report 00-455, available at http:// greenwood.cr.usgs.gov/pub/open-file-reports/ofr-00-0455/.

———2000b, Program BOMCRATR for crosswell radar and seismic tomography: U. S. Geological Survey Open-File Report 00-454, available at http:// greenwood.cr.usgs.gov/pub/open-file-reports/ofr-00-0454/.

———2000c, Program MIGRATOM for crosswell radar and seismic tomography: U. S. Geological Survey Open-File Report 00-457, available at http:// greenwood.cr.usgs.gov/pub/open-file-reports/ofr-00-0457/.

———2000d, Program 3DTOM for crosswell radar and seismic tomography: U. S. Geological Survey Open-File Report 00-456, available at http:// greenwood.cr.usgs.gov/pub/open-file-reports/ofr-00-0456/.

Vasco, D. W., J. E. Peterson Jr., and K. H. Lee, 1997, Ground-penetrating radar velocity tomography in heterogeneous and anisotropic media: Geophysics, **62**, 1758–1773.

Vasco, D. W., J. E. Peterson Jr., and E. L. Majer, 1996, A simultaneous inversion of seismic traveltimes and amplitudes for velocity and attenuation: Geophysics, **61**, 1738–1757.

———1998, Resolving seismic anisotropy—Sparse matrix methods for geophysical inverse problems: Geophysics, **63**, 970–983.

Wahl, J. S., 1983, Gamma-ray logging: Geophysics, **48**, 1536–1550.

Wänstdet, S., S. Carlsten, and S. Tirén, 2000, Borehole radar measurements aid structural interpretation: Journal of Applied Geophysics, 43, 227–237.

White, J. E., 1983, Underground sound, Application of seismic waves: Elsevier Science Publishing Co., Inc.

Williams, J. H., and C. D. Johnson, 2000, Borehole-wall imaging with acoustic televiewers for fractured-bedrock aquifer investigations: Proceedings of the 7th International Symposium on Borehole Geophysics for Minerals, Geotechnical, and Groundwater Applications, 43–53.

Williamson, P. R., 1993, Anisotropic crosshole tomography in layered media, Part 1—Introduction and methods: Journal of Seismic Exploration, **2**, 107–121.

———1998, On resolution and uniqueness in anisotropic crosshole traveltime tomography: Geophysics, **63**, 1184–1189.

Wong, J., 2000, Crosshole seismic imaging for sulfide orebody delineation near Sudbury, Ontario, Canada: Geophysics, **65**, 1900–1907.

Wright, D. L., J. D. Abraham, K. J. Ellefsen, and J. Rossabi, 1998, Borehole radar tomography and dielectric logging at the Savannah River Site: Proceedings of the Seventh International Conference on Ground-Penetrating Radar, 539–544.

Wright, D. L., R. D. Watts, and E. Bramsoe, 1984, A short-pulse electromagnetic transponder for hole-to-hole use: IEEE Transactions on Geoscience and Remote Sensing, **GE-22**, 720–725.

Wyllie, M. R. J., A. R. Gregory, and G. H. F. Gardner, 1958, An experimental investigation of factors affecting elastic wave velocities in porous media: Geophysics, **23**, 459–493.

Yamamoto, T., T. Nye, and M. Kuru, 1995, Imaging the permeability structure of a limestone aquifer by crosswell acoustic tomography: Geophysics, **60**, 1634–1645.

Zemanek, J., E. E. Glenn, L. J. Norton, and R. J. Caldwell, 1970, Formation evaluation by inspection with the borehole televiewer: Geophysics, **35**, 254.

Zhou, C., and L. Liu, 2000, Simultaneous inversion for velocity and attenuation, *in* D. Noon, G. Stickley, and D. Longstaff, eds., Proceedings of the 8th International Conference on Ground Penetrating Radar, electronic publication.

Zhou, C., G. T. Schuster, S. Hassanzadeh, and J. M. Harris, 1997, Elastic wave equation traveltime and waveform inversion of crosswell data: Geophysics, **62**, 853-868.